

1 Global Greenhouse Gas Reconciliation 2022

2 Zhu Deng^{1,2,3}, Philippe Ciais^{4,*}, Liting Hu⁵, Adrien Martinez⁴, Marielle Saunois⁴, Rona L. Thompson⁶,
3 Kushal Tibrewal⁴, Wouter Peters^{7,8}, Brendan Byrne⁹, Giacomo Grassi¹⁰, Paul I. Palmer^{11,12}, Ingrid T.
4 Luijkx⁷, Zhu Liu^{1,2,3,*}, Junjie Liu^{9,13}, Xuekun Fang⁵, Tengjiao Wang¹⁴, Hanqin Tian¹⁵, Katsumasa
5 Tanaka^{4,16}, Ana Bastos¹⁷, Stephen Sitch¹⁸, Benjamin Poulter¹⁹, Clément Albergel²⁰, Aki Tsuruta²¹,
6 Shamil Maksyutov¹⁶, Rajesh Janardanan¹⁶, Yosuke Niwa^{16,22}, Bo Zheng^{23,24}, Joël Thanwerdas²⁵, Dmitry
7 Belikov²⁶, Arjo Segers²⁷, Frédéric Chevallier⁴

8 ¹Department of Geography, University of Hong Kong, Hong Kong SAR, China

9 ²Institute for Climate and Carbon Neutrality, University of Hong Kong, Hong Kong SAR, China

10 ³Department of Earth System Science, Tsinghua University, Beijing, China

11 ⁴Laboratoire des Sciences du Climat et de l'Environnement, IPSL, CEA-CNRS-UVSQ, Université Paris-Saclay, Gif-sur-
12 Yvette, France

13 ⁵College of Environmental & Resource Sciences, Zhejiang University, Hangzhou, Zhejiang, China

14 ⁶Norwegian Institute for Air Research (NILU), Kjeller, Norway

15 ⁷Meteorology and Air Quality Department, Wageningen University & Research, Wageningen, the Netherlands

16 ⁸Energy and Sustainability Research Institute Groningen, University of Groningen, Groningen, the Netherlands

17 ⁹Jet Propulsion Laboratory, California Institute of Technology, Pasadena, CA, USA

18 ¹⁰Joint Research Centre, European Commission, Ispra (VA), Italy

19 ¹¹National Centre for Earth Observation, University of Edinburgh, Edinburgh, UK

20 ¹²School of GeoSciences, University of Edinburgh, Edinburgh, UK

21 ¹³Division of Geological and Planetary Sciences, California Institute of Technology, Pasadena, CA, USA

22 ¹⁴Institute of Blue and Green Development, Shandong University, Weihai, China

23 ¹⁵International Center for Climate and Global Change Research, School of Forestry and Wildlife Sciences, Auburn
24 University, Auburn, AL 36849, USA

25 ¹⁶Earth System Division, National Institute for Environmental Studies, Onogawa 16-2, Tsukuba, Ibaraki 305-8506, Japan

26 ¹⁷Institute for Earth System Science and Remote Sensing, Leipzig University, 04103 Germany

27 ¹⁸Faculty of Environment, Science and Economy, University of Exeter, Exeter, UK

28 ¹⁹NASA Goddard Space Flight Center, Biospheric Sciences Laboratory, Greenbelt, MD 20771, USA

29 ²⁰European Space Agency Climate Office, ECSAT, Harwell Campus, Didcot, Oxfordshire, UK

30 ²¹Finnish Meteorological Institute, P.O. Box 503, 00101, Helsinki, Finland

31 ²²Department of Climate and Geochemistry Research, Meteorological Research Institute (MRI), Nagamine 1-1, Tsukuba,
32 Ibaraki 305-0052, Japan

33 ²³Shenzhen Key Laboratory of Ecological Remediation and Carbon Sequestration, Institute of Environment and Ecology,
34 Tsinghua Shenzhen International Graduate School, Tsinghua University, Shenzhen, 518055, China

35 ²⁴State Environmental Protection Key Laboratory of Sources and Control of Air Pollution Complex, Beijing 100084, China

36 ²⁵Empa, Swiss Federal Laboratories for Materials Science and Technology, Dübendorf, Switzerland

37 ²⁶Center for Environmental Remote Sensing, Chiba University, Chiba, Japan

38 ²⁷TNO, Department of Air quality and Emissions Research, P.O. Box 80015, NL-3508-TA, Utrecht, the Netherland

39 *Correspondence to:* Philippe Ciais (philippe.ciais@lscce.ipsl.fr); Zhu Liu (zhuliu@hku.hk)

40 **Abstract.** In this study, we provide an update of the methodology and data used by Deng et al. (2022) to compare the
41 national greenhouse gas inventories (NGHGs) and atmospheric inversion model ensembles contributed by international

42 research teams coordinated by the Global Carbon Project. The comparison framework uses transparent processing of the net
43 ecosystem exchange fluxes of carbon dioxide (CO₂) from inversions to provide estimates of terrestrial carbon stock changes
44 over managed land that can be used to evaluate NGHGs. For methane (CH₄), and nitrous oxide (N₂O), we separate
45 anthropogenic emissions from natural sources based directly on the inversion results, to make them compatible with
46 NGHGs. Our global harmonized NGHGs database was updated with inventory data until February 2023 by compiling data
47 from periodical UNFCCC inventories by Annex I countries and sporadic and less detailed emissions reports by non-Annex I
48 countries given by National Communications and Biennial Update Reports. For the inversion data, we used an ensemble of
49 22 global inversions produced for the most recent assessments of the global budgets of CO₂, CH₄ and N₂O coordinated by
50 the Global Carbon Project with ancillary data. The CO₂ inversion ensemble in this study goes through 2021, building on our
51 previous report from 1990 to 2019, and includes three new satellite inversions compared to the previous study, and an
52 improved managed land mask. As a result, although significant differences exist between the CO₂ inversion estimates, both
53 satellite and in-situ inversions over managed lands indicate that Russia and Canada had a larger land carbon sink in recent
54 years than reported in their NGHGs, while the NGHGs reported a significant upward trend of carbon sink in Russia but a
55 downward trend in Canada. For CH₄ and N₂O, the results of the new inversion ensembles are extended to 2020. Rapid
56 increases in anthropogenic CH₄ emissions were observed in developing countries, with varying levels of agreement between
57 NGHGs and inversion results, while developed countries showed a slow declining or stable trend in emissions. Much denser
58 sampling of atmospheric CO₂ and CH₄ concentrations by different satellites, coordinated into a global constellation, is
59 expected in the coming years. The methodology proposed here to compare inversion results with NGHGs can be applied
60 regularly for monitoring the effectiveness of mitigation policy and progress by countries to meet the objective of their
61 pledges. The dataset constructed for this study is publicly available at <https://doi.org/10.5281/zenodo.13887128>, (Deng et al.,
62 2024).

删除[Zhu Deng]: 4

删除[Zhu Deng]: Much denser sampling and higher atmospheric CO₂ and CH₄ concentrations by different satellites, are expected in the coming years.

删除[Zhu Deng]: <https://doi.org/10.5281/zenodo.10841716>

63 **1 Introduction**

64 If modeled pathways align with Nationally Determined Contributions (NDCs) declared prior to COP26 (in 2021) until 2030
65 and do not involve any subsequent increase in ambition, the projected global warming by 2100 would be 2.1-3.4°C (IPCC,
66 2023). The global stocktake coordinated by the secretariat of the United Nations Framework Convention on Climate Change
67 (UNFCCC) considers data from national greenhouse gas inventories (NGHGs) to assess the collective climate progress to
68 curb emissions. It is expected there will be differences in the quality of NGHGs being reported to the UNFCCC (Perugini et
69 al., 2021). UNFCCC Annex I Parties, which include all OECD (Organisation for Economic Co-operation and Development)
70 countries and several EIT (Economies In Transition) already report annually their emissions following the same IPCC
71 guidelines (IPCC 2006) in a common reporting format, with a time latency of roughly 1.5 years. In contrast, non-Annex I
72 Parties, mostly developing and less developed countries, are currently not required to provide reports as regularly and as
73 detailed as Annex I Parties and in a few cases use different IPCC Guidelines in their National Communications (NC) or

74 Biennial Update Reports (BUR) submitted to the UNFCCC. Non-Annex I Parties are scheduled in 2024 to move to regular
75 and harmonized reporting of their emissions in the national inventory reports (NIRs) in the format of common reporting
76 tables (CRTs), following the Paris Agreement's enhanced transparency framework (ETF).

77 The IPCC guidelines for NGHGs encourage countries to use independent information to verify emissions and removals
78 (IPCC, 1997, 2006, 2019), such as comparisons with independently compiled inventory databases (e.g. IEA, CDIAC,
79 EDGAR, FAOSTAT), or with atmospheric mole fraction measurements interpreted by atmospheric inversion models (see
80 Section 6.10.2 in IPCC (2019)). Such verification of 'bottom-up' national reports against 'top-down' atmospheric inversion
81 results is not mandatory. However, a few countries (e.g. Switzerland, United Kingdom, New Zealand, and Australia) have
82 already added inversions as a consistency check of their national reports. In our study, we utilized the latest global inversion
83 results from the budget assessments of CO₂, CH₄, and N₂O conducted by the Global Carbon Project (GCP), focusing on
84 three ensembles of inversions with global coverage. Compared to our previous study (Deng et al., 2022), the CO₂ inversion
85 ensemble used in this study has been updated to the global CO₂ budget of Friedlingstein et al. (2022) that includes nine CO₂
86 inversions using mole fraction data from the surface network and/or retrieval products from the Greenhouse Gases
87 Observing Satellite (GOSAT) and Orbiting Carbon Observatory-2 (OCO-2) satellites. The CH₄ inversion ensemble and N₂O
88 inversion (Tian et al., 2023) ensemble used in this study are also extended to the 2020. As a result, the new ensembles cover
89 up to 2021 for CO₂, 2020 for CH₄ and 2020 for N₂O, compared to 2019, 2017 and 2016 respectively in our previous study
90 (Deng et al., 2022), allowing us to track and analyze the most recent flux variations.

91 Our framework to process the inversion data aims at making them comparable to inventories at countries or groups of
92 countries scale (ie,with an area larger than the spatial resolution of atmospheric transport models typically used for
93 inversions). Atmospheric inversions use *a priori* information for the spatial and temporal patterns of fluxes. Some inversions
94 correct prior fluxes at the spatial resolution of their transport models to match atmospheric observations and use spatial error
95 correlations (usually e-folding length scales) that tie the adjustment of fluxes from one grid cell to its neighbors at distances
96 of tens to hundreds of kilometers. Other inversions adjust fluxes over coarse regions that are larger than the resolution of the
97 transport model, implicitly assuming a perfect correlation of flux errors within these regions, causing an aggregation error
98 (Kaminski et al., 2001). Thus, to minimize aggregation errors, the results of inversions are shown preferentially for selected
99 large area emitter countries or large absorbers in the case of CO₂. We have selected a different set of countries or groups of
100 countries for each gas, according to their importance in the global emission budget. According to the median of inversion
101 data we used in this study, selected countries collectively represent ~70% of global fossil fuel CO₂ emissions, ~90% of
102 global land CO₂ sink, ~60% of anthropogenic CH₄ emissions, and ~55% of anthropogenic N₂O emissions (Fig S1). To
103 more robustly interpret global inversion results for comparison with inventories, we follow the same criterion and choose
104 high-emitting countries covered (if possible) by atmospheric measurements, although most selected tropical countries have
105 few or no atmospheric in-situ stations. Uncertainties are given by the spread among inversion models (min-max range given
106 the small number of inversions), and the causes for discrepancies with inventories are analyzed systematically and on a case-

删除[Ana Bastos]: /

107 by-case basis, considering both individual countries and specific greenhouse gases, for annual variations and for mean
108 budgets over several years.

109 Based on the newly updated inversion results and inventory, and an improvement in the methodology framework proposed
110 in the previous study (Deng et al., 2022), we specifically address the following questions: 1) how do inversion models
111 compare with NGHGs for the three gases?; 2) what are the plausible reasons for mismatches between inversions and
112 NGHGs?; 3) did the new maps of managed land masks in this study reduce the mismatch between the inversions and
113 NGHGs for CO₂ and N₂O?; 4) what independent information can be extracted from inversions to evaluate the mean values
114 or the trends of greenhouse gas emissions and removals?; 5) does this information exhibit a good agreement with NGHGs?;
115 and 6) how do satellite-retrieval driven inversion models differ from the surface in-situ and flask sampling driven inversion
116 model results?

删除[Liting Hu]: and in particular,

删除[Liting Hu]: 3

删除[Liting Hu]: and

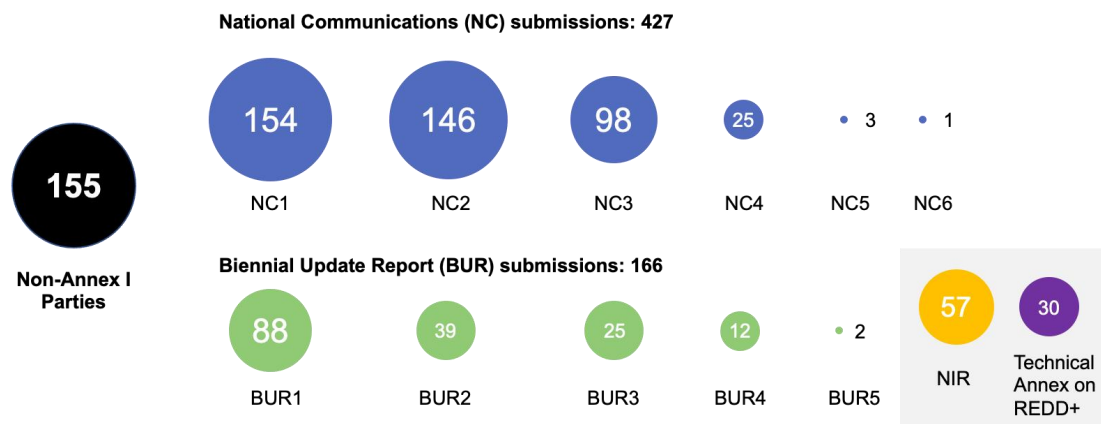
删除[Liting Hu]: 4

117 Sections 2 presents the updated global database of national emissions reports for selected countries and its grouping into
118 sectors, the global atmospheric inversions used for the study, the processing of fluxes from these inversions to make their
119 results as comparable as possible with inventories. The time series of inversions compared with inventories for each gas,
120 with insights on key sectors for CH₄ are discussed in **Sections 3 to 5**. The discussion (Section 6) focuses on the plausible
121 reasons for mismatches between inversions and NGHGs, comparison between inversion ensembles in this study and
122 previous study, and different priors applied in the CH₄ inversions. Finally, concluding remarks are drawn on how inversions
123 could be used systematically to support the evaluation and possible improvement of inventories for the Paris Agreement.

124 **2 Material and methods**

125 **2.1 Compilation and harmonization of national inventories reported to the UNFCCC**

126 All UNFCCC Parties shall periodically update and submit their national GHG inventories of emissions by sources and
127 removals by sinks to the Convention parties. Annex I countries submit their NIRs in common reporting format (CRF) tables
128 every year with a complete time series starting in 1990. Non-Annex I Parties are required to submit their NC roughly every
129 four years after entering the Convention and submit BUR, every two years since 2014. Currently, there are in total 427
130 submissions of NC and over 166 submissions of BUR (UNFCCC, 2021b, a) (**Fig 1**).



131

132

133

134

135

136

137

138

139

140

141

142

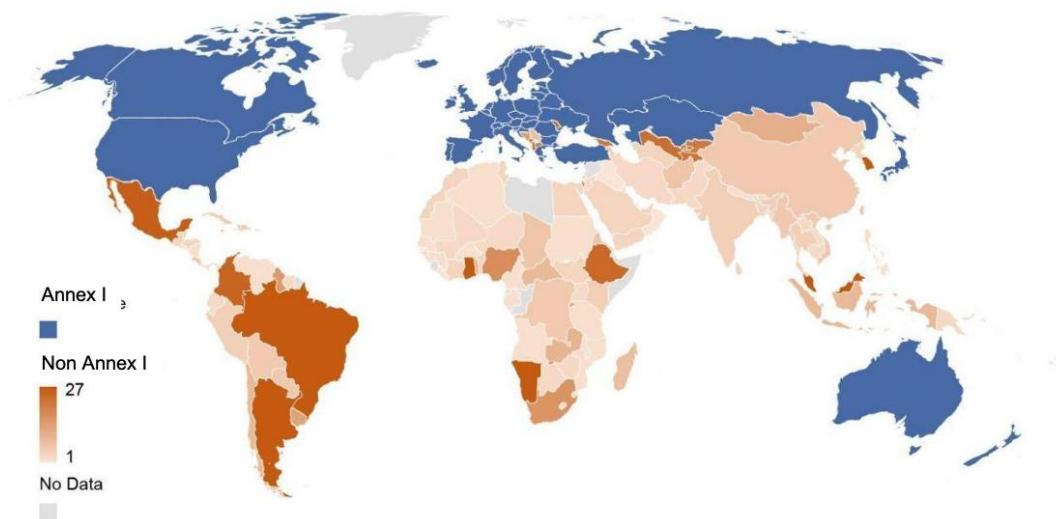
143

144

145

Figure 1. Numbers of non-Annex I parties for each submission round (as of February 28, 2023). The numbers in the middle of the dots denote the numbers of non-Annex I parties for each submission, while the black dots denote the total number of non-Annex I parties, the blue dots denote the numbers of non-Annex I parties who has submitted National Communications (NC), green dots for Biennial Update Reports (BUR), yellow dots for National Inventory Report (NIR), and purple dots for Technical Annex on REDD+ . The numbers after the NC and BUR denote the total number of submission reports.

We collected NGHGI data submitted to UNFCCC by February 28, 2023. For Annex I countries, data collection is straightforward, as their reports are provided as Excel files under a Common Reporting Format (CRF) until the year 2020 last accessed on February 28, 2023. For non-Annex I countries, the data were directly extracted from the original reports provided in Portable Document Format (PDF) last accessed on February 28, 2023. Data from successive reports for the same country were extracted, except when they relate to the same years, in which case only the latest version is considered. While Annex I countries are required to compile their inventory following IPCC 2006 guidelines and the subdivision between sectors established by the UNFCCC decision (dec. 24/CP.19), non-Annex I countries are increasingly adopting the IPCC 2006 Guidelines, although some still utilize the older IPCC 1996 Guidelines, with different approaches and sectors. Consequently, the methods used and the reported sectors may differ among NC and BUR reports.



146

147 **Figure 2. Number of years covered by NGHGI reports (NC+BUR) in each non-Annex I country (as of February 28, 2023).**

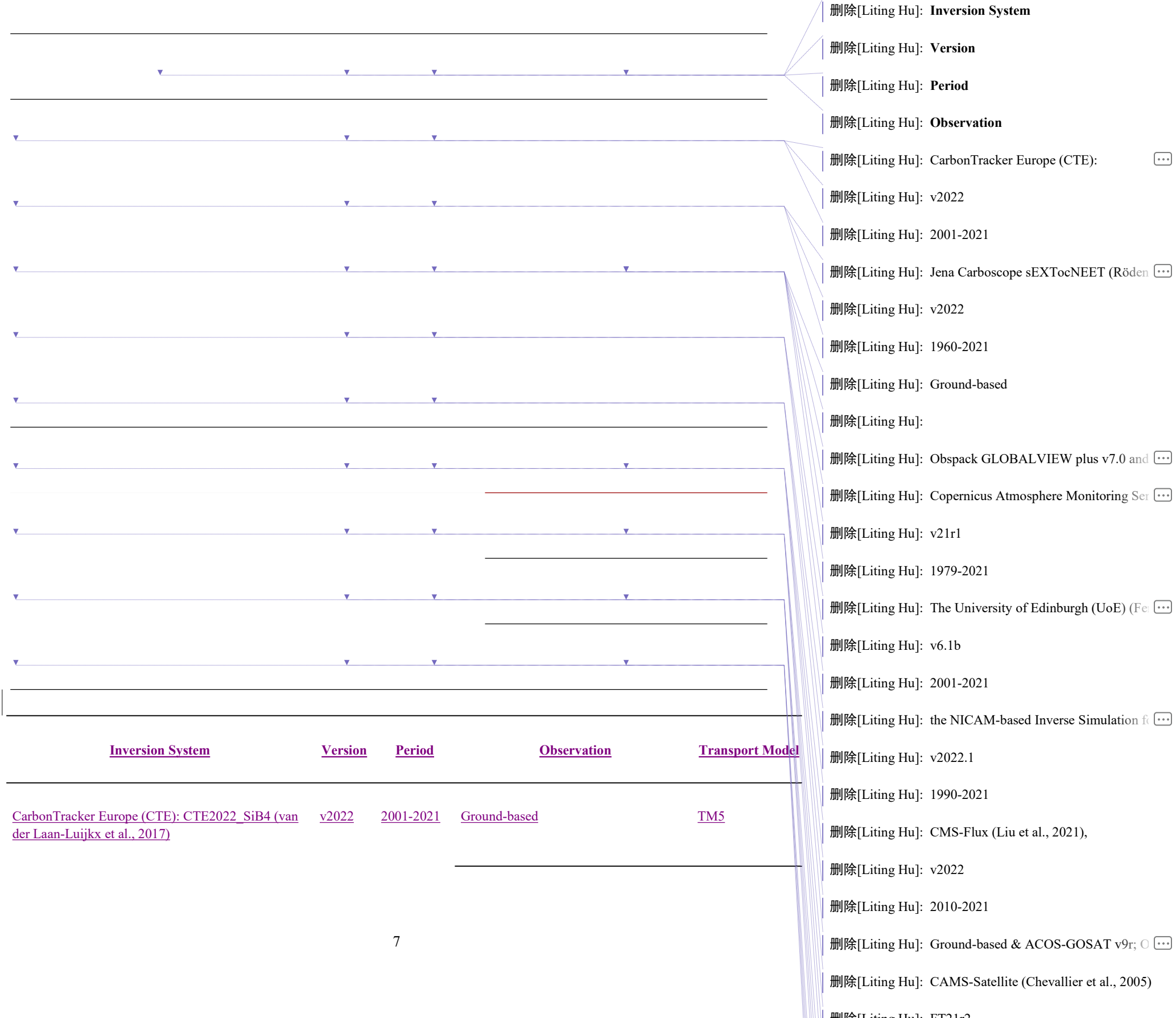
148 Emissions from Greenland are reported by Denmark.

149 2.2 Atmospheric inversions

150 CO₂ inversions



151 Nine CO₂ inversion systems from the 2022 Global Carbon Budget of the GCP (Friedlingstein et al., 2022) are used,
 152 including CarbonTracker-Europe (CTE) v2022 (van der Laan-Luijkx et al., 2017), Jena Carboscope v2022 (Rödenbeck et al.,
 153 2003), the surface air-sample inversion from the Copernicus Atmosphere Monitoring Service (CAMS) v21r1 (Chevallier et
 154 al., 2005), the inversion from the CAMS Satellite FT21r2 (Chevallier et al., 2005), the inversion from the University of
 155 Edinburgh (UoE) v6.1b (Feng et al., 2016), the NICAM-based Inverse Simulation for Monitoring CO₂ (NISMON-CO₂)
 156 v2022.1 (Niwa et al., 2022), CMS-Flux v2022 (Liu et al., 2021), GONGGA v2022 (Jin et al., 2023), and THU v2022 (Kong
 157 et al., 2022). A variety of transport models are used by these systems, which allows for representing a major driver factor
 158 behind differences in flux estimates based on atmospheric inversions, particularly their distribution over latitudinal bands.
 159 Among the nine inversions, four systems (CAMS Satellite FT21r2, GONGGA v2022, THU v2022, and CMS-Flux v2022)
 160 utilize satellite CO₂ column retrievals from GOSAT and/or OCO-2, calibrated to the World Meteorological Organization
 161 (WMO) 2019 standards. CMS-Flux additionally incorporates in-situ observed CO₂ mole fraction records. The remaining five
 162 inversion systems (CAMS v21r1, CTE v2022, Jena Carboscope v2022, UoE v6.1b, and NISMON-CO₂ v2022.1) solely rely
 163 on CO₂ mole fractions that were observed in-situ or collected in flasks (Schuldt et al., 2021, 2022). The CO₂ inversion
 164 records extend up to and including 2021. Their flux estimates are available at [https://meta.icos-](https://meta.icos-cp.eu/objects/GahdRITjT22GGmq_GCi4o_wy)
 165 [cp.eu/objects/GahdRITjT22GGmq_GCi4o_wy](https://meta.icos-cp.eu/objects/GahdRITjT22GGmq_GCi4o_wy) and details are summarized in **Table 1**.

166 **Table 1 | Atmospheric CO₂ inversions used in this study** (Friedlingstein et al., 2022)



Jena CarboScope sEXTocNEET (Rödenbeck et al., 2003)	v2022	1960-2021	Obspack GLOBALVIEW plus v7.0 and NRT_v7.2	TM3
Copernicus Atmosphere Monitoring Service (CAMS) (Chevallier et al., 2005)	v21r1	1979-2021		LMDZ v6
The University of Edinburgh (UoE) (Feng et al., 2016)	v6.1b	2001-2021		GEOS-CHEM
the NICAM-based Inverse Simulation for Monitoring CO2 (NISMON-CO2) (Niwa et al., 2022)	v2022.1	1990-2021		NICAN-TM
CMS-Flux (Liu et al., 2021)	v2022	2010-2021	Ground-based & ACOS-GOSAT v9r; OCO-2 v10 scaled to WMO2019	GEOS-CHEM
CAMS-Satellite (Chevallier et al., 2005)	FT21r2	2010-2021	bias-corrected ACOS GOSAT v9 over land until August 2014 + bias-corrected ACOS OCO-2 v10 over land, both rescaled to WMO2019	LMDZ v6
THU (Kong et al., 2022)	v2022	2015-2021	OCO-2 v10r data scaled to WMO2019	GEOS-CHEM
GONGGA (Jin et al., 2023)	v2022	2015-2021	OCO-2 v10r data scaled to WMO2019	GEOS-CHEM

168 CH₄ inversions

169 The CH₄ emissions come from the new ensemble of inversions (Saunois et al. [2024](#) ) from 2000 to 2020, using seven
170 different inverse systems for a total nine inversions (**Table 2**). The inverse systems include: CarbonTracker-Europe CH₄
171 (Tsuruta et al., 2017), LMDZ-PYVAR (Yin et al., 2015; Zheng et al., 2018), CIF-LMDZ(Berchet et al., 2021), MIROC4-
172 ACTM (Patra et al., 2018; Chandra et al., 2021), NISMON-CH₄ (Niwa et al., 2022), NIES-TM-FLEXPART (Maksyutov et
173 al., 2021; [Janardanan et al., 2024](#)), and TM5-CAMS (Segers and Houweling, 2017). This ensemble of inversions gathers
174 various chemistry transport models, differing in vertical and horizontal resolutions, meteorological forcing, advection  and

删除[Zhu Deng]: in prep.

删除[Shamil]: Wang et al., 2019;

175 convection [\(vertical transport\)](#) schemes, and boundary layer mixing [_](#). Including these different systems is a conservative
 176 approach that allows to cover different potential uncertainties of the inversion, among them: model transport, set-up issues,
 177 and prior dependency. [All inversions except two, use updated common prior emission maps for natural and anthropogenic](#)
 178 [prior emissions divided into 12 sectors, particularly the EDGAR v6 inventory for prior fossil fuel emissions \(Crippa et al.,](#)
 179 [2021a extrapolated to Jan 1st, 2021\), GFED for fires and ecosystem models for wetland emissions. During the production of](#)
 180 [the inversion simulations, \[GAINS inventory \\(Höglund-Isaksson, 2013\\)\]\(#\),](#) was proposed to use another prior for fossil fuel
 181 [sources,](#) instead of [using EDGAR v6](#) (see Supplementary Text 3 in Saunio et al, 2024). GAINS has higher fossil emissions,
 182 in particular over the US and a higher increase of fossil emissions over time in the US (Tibrewal et al., 2024). As Tibrewal et
 183 al. showed that inversions are strongly attracted to their priors, comparison between results with GAINS and EDGAR v6
 184 priors is informative about how robust are inversions to their priors when they are used to ‘verify’ NGHGs. Some inversions
 185 optimize emissions in groups of sectors, and others only provide total gridded emissions [\(MIROC4-ACTM and TM5-CAMS,](#)
 186 [details can be found in Table S10 in Saunio et al, 2024\)](#). For the latter, we computed the emission from each sector within
 187 each pixel based on the proportion of the prior fluxes. [Such processing can lead to significant uncertainties if not all sources](#)
 188 [increase or change at the same rate in a given region/pixel.](#) The inversions assimilating surface stations mole fraction
 189 observations provide results since 2000, and those assimilating satellite observations from column CH₄ measurements
 190 (XCH₄) of the GOSAT satellite provide results since 2010, first full year of GOSAT observations. Inversion results were
 191 gridded into 1° by 1° monthly emission maps and aggregated nationally using a country mask (Klein Goldewijk et al., 2017).

删除[Zhu Deng]:

删除[Zhu Deng]: it

删除[Zhu Deng]: GAINS inve

删除[Zhu Deng]: ntor

删除[Zhu Deng]: Höglund-Isaksson

删除[Zhu Deng]: IIASA

删除[Zhu Deng]: 20

删除[Zhu Deng]: 13

删除[Liting Hu]: REF

192 **Table 2 | Atmospheric CH₄ inversions used in this study (Saunio et al 2024)**

删除[Zhu Deng]: . in prep.

Inversion system	Abbreviation	Institution	Observations	Period
Carbon Tracker-Europe CH ₄	CTE	FMI	Surface stations	2000-2020
CIF-LMDz	CIF-LMDz	LSCE/CEA	Surface stations	2000-2020
LMDz-PYVAR	PYVAR-LMDz	LSCE/CEA	GOSAT Leicester v7.2	2010-2020
MIROC4-ACTM	MIROC4-ACTM	JAMSTEC	Surface stations	2000-2020
NISMON-CH ₄	NISMON-CH ₄	NIES/MRI	Surface stations	2000-2020

NIES-TM-FLEXPART (NTF)	NIES	NIES	Surface stations	2000-2020
NIES-TM-FLEXPART (NTF)	NIES	NIES	Surface + GOSAT NIES L2 v02.95	2010-2020
TM5-CAMS	TM5	TNO/VU	Surface stations	2000-2020
TM5-CAMS	TM5	TNO/VU	GOSAT ESA/CCI v2.3.8 (combined with surface observations)	2010-2020

193 **N₂O inversions**

194 Four N₂O inversion systems from the updated GCP Nitrous Oxide Budget (Tian et al., 2023) are used: INVICAT (Wilson et
 195 al., 2014), PyVAR-CAMS (Thompson et al., 2014), MIROC4-ACTM (Patra et al., 2018, 2022) and GEOS-Chem (Wells et
 196 al., 2015). The N₂O inversion results are updated up to 2020.

197 **Table 3 | Atmospheric N₂O inversions used in this study** (Tian et al., 2023)

Inversion system	Institution	Period
INVICAT (Wilson et al., 2014)	Univ. Leeds	1995-2020
PyVAR-CAMS (Thompson et al., 2014),	NILU/LSCE	1995-2020
MIROC4-ACTM (Patra et al., 2018, 2022)	JAMSTEC	1997-2019
GEOS-Chem (Wells et al., 2015)	Univ. Minnesota	1995-2019

198 **Aggregating the gridded inversion results into national totals**

199 To obtain national annual-scale flux estimates, we aggregated the gridded flux maps of each inversion with various native
200 resolutions following the methodology outlined in Chevallier (2021). This involved using the $0.08^\circ \times 0.08^\circ$ land country
201 mask of Klein Goldewijk et al. (2017) to calculate the fraction of each country in each inversion grid box.

202 **2.3 Processing of CO₂ inversion data for comparison with NGHGs**

203 **Fossil fuel emissions re-gridding - managed land mask**

204 To analyze terrestrial CO₂ fluxes, we subtracted the same fossil fuel emissions (including cement) of GridFEDv2022.2
205 (Jones et al., 2022) from the total CO₂ flux of each inversion. This is equivalent to assuming perfect knowledge of fossil
206 emissions, adding up to a global total of 9.7 GtC/yr for the year 2021. The dataset used national annual emissions estimates
207 from the 2022 global carbon budget (Friedlingstein et al., 2022) which uses the reported NGHGs data from Annex I
208 countries and are assumed to be broadly consistent with the non-Annex I countries. This assumption may lead to
209 underestimating the uncertainty of terrestrial CO₂ fluxes deduced from inversions.

210 As defined in the IPCC Guidelines for NGHGs (IPCC, 2006), only CO₂ emissions and removals from managed land are
211 reported in NGHGs as a proxy for human-induced effects (direct effects and indirect effects such as CO₂ fertilization and
212 nitrogen deposition). However, inversion models retrieve all CO₂ fluxes (due to both direct and indirect effects, plus the
213 natural interannual variability) over all lands. We thus retained inversions' national estimates of the Net Ecosystem
214 Exchange (NEE) CO₂ flux ($F_{ML}^{inv\ NEE}$) over managed lands grid cells only (*ML*, here defined as all land except intact forests)
215 because the fluxes over unmanaged land are not counted by NGHGs. We use NEE from the definition of Ciais et al. (2020),
216 representing all non-fossil CO₂ exchange fluxes between terrestrial surfaces and the atmosphere. Other work may use Net
217 Biome Production (NBP) with a similar meaning. CO₂ fluxes over unmanaged lands were excluded from the terrestrial CO₂
218 flux totals that will be compared with NGHGs, proportional to their presence in each inversion grid box. The new maps of
219 non-intact forests are compiled by Grassi et al. (2023). These maps include official country-managed forest and other
220 managed land areas for Canada and Brazil used for their NGHGs, and the intact forest map (Potapov et al., 2017) as a
221 substitute for unmanaged land where country-based information is not available. For Russia, we used non-intact forest maps
222 for each province with thresholds adjusted to match the official managed land areas from Russia's NIRs, and assumed that all
223 grasslands were managed. This approach assumes that non-intact forest areas can serve as a reasonably good proxy for
224 managed forests reported in the NGHGs (Grassi et al., 2021, 2023). It is important to note that this approach is somewhat
225 arbitrary, as highlighted in previous studies (Ogle et al., 2018; Chevallier, 2021; Grassi et al., 2021). However, in the
226 absence of a machine-readable definition of managed plots in many NGHGs, there is currently no better alternative
227 available.

228 Adjusting CO₂ fluxes due to lateral carbon transport by crop and wood products trade and by rivers

229 In addition to the extraction of **fossil CO₂ flux and** managed land CO₂ flux, there are CO₂ fluxes that are part of $F_{ML}^{inv NEE}$ but
230 are not counted by NGHGs. These fluxes are induced by (i) soils to rivers to oceans carbon export (F_{ML}^{rivers}) which has an
231 anthropogenic and a natural component (Regnier et al., 2013), and (ii) net anthropogenic export of crop and wood products
232 across each country's boundary ($F_{ant}^{crop trade}$ and $F_{ant}^{wood trade}$). The magnitudes of these CO₂ fluxes are different between
233 countries, and values from the selected countries are presented in **Fig S2**. We assume that NGHGs include CO₂ losses from
234 fire (wildfire and prescribed fire) and other disturbances (wind, pests) and from domestic harvesting, as recommended by the
235 IPCC reporting guidelines (IPCC, 2006, 2019) (although some countries, such as Canada and Australia exclude some
236 emissions from these disturbances, and the subsequent removals from the same areas (Grassi et al., 2023)). The adjusted
237 inversion NEE that can be compared with inventories, $F_{adj}^{inv NEE}$, is given by:

$$238 F_{adj}^{inv NEE} = F_{ML}^{inv NEE} - F_{ML}^{rivers} - F_{ant}^{crop trade} - F_{ant}^{wood trade} \Leftrightarrow F_{ant-nf}^{ni}, \quad (1)$$

239 where the sign \Leftrightarrow means 'compared with', F_{ant-nf}^{ni} is the **non-fossil part of the** anthropogenic CO₂ flux from NGHGs,
240 F_{tot}^{rivers} is the sum of the natural and anthropogenic CO₂ flux on land from CO₂ fixation by plants that is leached as carbon via
241 soils and channeled to inland waters to be exported to the ocean or to another country. All countries export river carbon, but
242 some countries also receive river inputs, e.g., Romania receives carbon from Serbia via the Danube River. We estimated the
243 lateral carbon export by rivers minus the imports from rivers entering each country, including dissolved organic carbon,
244 particulate organic carbon and dissolved inorganic carbon of atmospheric origin distinguished from lithogenic, by using the
245 data and methodology described by Ciais et al. (2021). Data are from Mayorga et al. (2010) and Hartmann et al. (2009) and
246 follow the approach of Ciais et al. (2021) proposed for large regions. We also extracted the lateral flux by rivers over the
247 managed land by using the same methodology as inversion CO₂ flux. Thus, in a country that only exports river carbon to the
248 ocean, the amount of carbon exported is equivalent to an atmospheric CO₂ sink, denoted as F_{ML}^{rivers} as in eq. (1), thus ignoring
249 burial, which is a small term. Over a country that receives carbon from rivers flowing into its territory, a small national CO₂
250 outgassing is produced by a fraction of this imported flux. In that case, we assumed that the fraction of outgassed to
251 incoming river carbon is equal to the fraction of outgassed to soil-leached carbon in the RECCAP2 region to which a country
252 belongs, estimated with data from Ciais et al. (2021).

253 $F_{ant}^{crop trade}$ is the sum of CO₂ sinks and sources induced by the trade of crop products. This flux was estimated from the
254 annual trade balance of crop commodities calculated for each country from data from the United Nations Statistics Division
255 of the Food and Agriculture Organization (FAOSTAT) combined with the carbon content values of each commodity (Xu et
256 al., 2021). All the traded carbon in crop commodities is assumed to be oxidized as CO₂ in one year, neglecting stock changes
257 of products, and the fraction of carbon from crop products going to waste pools and sewage waters after consumption, thus
258 not necessarily oxidized to atmospheric CO₂. $F_{ant}^{wood trade}$ is the sum of CO₂ sinks and sources induced by the trade of wood
259 products (Zscheischler et al., 2017). Here, we followed Ciais et al. (2021) who used a bookkeeping model to calculate the

删除[Zhu Deng]: SI

删除[Zhu Deng]: 1

fraction of domestically produced and imported carbon in wood products that are oxidized in each country during subsequent years, with product lifetimes defined by Mason Earles et al (2012) and encompassing all products (including roundwood and processed products). The underlying assumption in estimating CO₂ fluxes from wood harvest is that the emissions from domestically harvested wood, in addition to imported wood minus exported wood that is not allocated to wood product pools, are released into the atmosphere during the year of harvest. Conversely, wood allocated to wood product pools is gradually released into the atmosphere over time, based on their respective lifetimes. Domestic harvest is assumed to be balanced by an atmospheric CO₂ sink of equivalent magnitude, which is not necessarily the case given that harvest is rarely in equilibrium with forest increment, but inversions NEE will correct for this imbalance in our results, and can thus be compared with NGHGs. We included in the $F_{ant}^{crop\ trade}$ flux the emissions of CO₂ by domestic animals consuming specific crop products delivered as feed. On the other hand, emissions of CO₂ from grazing animals and the decomposition of their manure are supposed to occur in the same grid box where grass is grazed, so that the CO₂ net flux captured by an inversion is comparable with grazed grasslands' carbon stock changes of inventories. Emissions of reduced carbon compounds (VOCs, CH₄, CO) are not included in this analysis (see Ciais et al. (2021) for a discussion of their importance in inversion CO₂ budgets).

In summary, the purpose of the adjustment of eq. (1) is to make inversion output comparable to the NGHGs that do not include F_{ML}^{rivers} , $F_{ant}^{crop\ trade}$ and $F_{ant}^{wood\ trade}$. The UNFCCC accounting rules (IPCC, 2006) assume that all the harvested wood products are emitted in the territory of a country that produces them, which is equivalent to ignoring $F_{ant}^{wood\ trade}$ as a national sink or source of CO₂, hence the need to remove $F_{ant}^{wood\ trade}$ from inversion NEE. The adjusted inversion fluxes from eq. (1) depict the national CO₂ stock change which match better the carbon accounting system boundaries of UNFCCC NGHGs. In the following, we will only discuss adjusted inversion CO₂ fluxes ($F_{adj}^{inv\ NEE}$), but for simplicity call them “inversion fluxes”.

2.4 Processing of CH₄ inversions for comparison with national inventories

Most atmospheric inversions derive total net CH₄ emissions at the surface as it is difficult for them to disentangle overlapping emissions from different sectors at the pixel/regional scale based on atmospheric CH₄ observations only. However, five of the seven inverse systems solve for some source categories owing to different spatio-temporal distributions between the sectors. For each inversion, monthly gridded posterior flux estimates were provided at 1°x1° grid resolution for the net flux at the surface (E_{net}^{inv}), the soil uptake at the surface (E_{soil}^{inv}), the total emission at the surface (E_{tot}^{inv}) and five emitting ‘super sectors’ which regroup several IPCC sectors: Agriculture & Waste (E_{AgW}^{inv}), Fossil Fuel (E_{FF}^{inv}), Biomass & Biofuel Burning (E_{BB}^{inv}), Wetlands (E_{Wet}^{inv}), and Other Natural (E_{Oth}^{inv}) emissions. Considering the soil uptake as a ‘negative source’ given separately, the following equations apply:

$$E_{net}^{inv} = E_{tot}^{inv} + E_{soil}^{inv} = E_{AgW}^{inv} + E_{FF}^{inv} + E_{BB}^{inv} + E_{Wet}^{inv} + E_{Oth}^{inv} + E_{soil}^{inv} \quad (2)$$

For inversions solving for net emissions only, the partition to source sectors was created based on using a fixed ratio of sources calculated from prior flux information at the pixel scale. For inversions solving for some categories, a similar

approach was used to partition the solved categories to the five aforementioned emitting sectors. Such processing can lead to significant uncertainties if not all sources increase or change at the same rate in a given region/pixel. National values have been estimated using the country land mask described in the CO₂ section, thus offshore emissions are not counted as part of inversion results unless they are in a coastal grid cell.

In our previous study (Deng et al., 2022), four methods were proposed to separate CH₄ anthropogenic emissions from inversions (E_{Anth}^{inv}) to compare them with national inventories (E_{Anth}^{ni}) aiming to discuss the uncertainties in anthropogenic CH₄ emissions associated with the chosen separation methods. These four methods include: (1) summing prior estimates based on inversions for anthropogenic sectors (method 1); (2) subtracting natural emissions from total fluxes (method 2); and (3) subtracting natural emissions derived from other bottom-up assessments from the total inversion flux (methods 3/1 and 3/2, differing only in the bottom-up wetland CH₄ data used). The calculations of anthropogenic emissions by each method were performed separately for GOSAT inversions and in-situ inversions. However, the uncertainty from the separation method is generally much smaller than the variability between different inversion models (see Deng et al. (2022) Fig 9). Therefore, we apply only one method in this study which consists of using inversion partitioning as defined in Saunio et al. (2020):

$$E_{Anth}^{inv} = E_{AgW}^{inv} + E_{FF}^{inv} + E_{BB}^{inv} - E_{wildfires}^{BU} \Leftrightarrow E_{Anth}^{ni} \quad (3)$$

This method has some uncertainties. First, the partitioning relies on prior fractions within each pixel, and second, emissions from wildfires are counted for in the Biomass and Biofuel burning (*BB*) inversion category while they are not necessarily reported in NGHGs. The *BB* inversion category includes methane emissions from wildfires in forests, savannahs, grasslands, peats, agricultural residues, and the burning of biofuels in the residential sector (stoves, boilers, fireplaces). Therefore, we subtracted bottom-up (*BU*) emissions from wildfires ($E_{wildfires}^{BU}$) based on the GFEDv4 dataset (van Wees et al., 2022) using their reported dry matter burned and CH₄ emission factors. Because the GFEDv4 dataset also reports specific agricultural and waste fire emissions data, we assumed that those fires (on managed lands) are reported by NGHGs, so they were not counted in $E_{wildfires}^{BU}$. Figure S3 presents a comparison between our adjusted *BB* flux and the wood fuel emissions reported by Flammi et al. (2023). This comparison highlights the broader scope and definition of our adjusted *BB* flux, illustrating the differences in emissions estimation methodologies.

2.5 Processing of N₂O inversions for comparison with inventories

We subtracted estimates of natural N₂O sources from the N₂O emission budget (E_{tot}^{inv}) of each inversion, to provide inversions of anthropogenic emissions (E_{ant}^{inv}) that can be compared with national inventories (E_{ant}^{ni}):

$$E_{ant}^{inv} = E_{ML}^{inv} - E_{nat}^{aq} - E_{wildfires}^{GFED} \Leftrightarrow E_{ant}^{ni} \quad (4)$$

Here, the natural N₂O sources include natural emission from freshwater systems (E_{nat}^{aq}) and natural emissions from wildfires (E_{ant}^{ni}).

删除[Zhu Deng]: .

删除[Zhu Deng]: the differences in the calculated results among the four methods were smaller compared to the variations observed in the inversions

323 In our previous study, intact forest grid cells (assumed unmanaged) from Potapov et al. (2017) and lightly grazed grassland
324 areas from Chang et al. (2021) were removed from the gridded N₂O emissions in proportion to their presence in each
325 inversion grid box. Here we used the new managed land mask defined in **Section 2.3** to filter gridded N₂O emissions from
326 inversions to obtain E_{ML}^{inv} . We verified that the inversion grid box fractions classified as unmanaged do not contain point
327 source emissions from the industry, energy, and diffuse emissions from the waste sector, to make sure that we do not
328 inadvertently remove anthropogenic sources by masking unmanaged pixels. From the EDGARv4.3.2 inventory (Janssens-
329 Maenhout et al., 2019), we found that N₂O from wastewater handling covers a relatively large area that might be partly
330 located in unmanaged land. But the corresponding emission rates are more than 1 order of magnitude smaller than those
331 from agricultural soils. For other sectors, only very few of the unmanaged grid boxes contain point sources, and none of
332 them have an emission rate that is comparable with agricultural soils (managed land). Thus, our assumption that emissions
333 from these other anthropogenic sectors are primarily over managed land pixels is solid (other sectors include: the power
334 industry; oil refineries and transformation industry; combustion for manufacturing; aviation; road transportation no
335 resuspension; railways, pipelines, off-road transport; shipping; energy for buildings; chemical processes; solvents and
336 products use; solid waste incineration; wastewater handling; solid waste landfills).

337 The flux E_{nat}^{aq} is the natural emission from freshwater systems given by a gridded simulation of the DLEM model (Yao et al.,
338 2019) describing pre-industrial N₂O emissions from N leached by soils and lost to the atmosphere by rivers in the absence of
339 anthropogenic perturbations (considered as the average of 1900-1910). Natural emissions from lakes were estimated only at
340 a global scale by Tian et al. (2020), and represent a small fraction of rivers' emissions. Therefore, they are neglected in this
341 study. The flux $E_{wildfires}^{GFED}$ is based on the GFED4s dataset (van Wees et al., 2022) using their reported dry matter burned and
342 N₂O emission factors. Because the GFED dataset reports specific agricultural and waste fire emissions data, we assume that
343 those fires (on managed lands) are reported by NGHGs so they were not counted in $E_{wildfires}^{GFED}$ just like for CH₄ emissions.
344 Note that there could also be a background natural N₂O emission from natural soils over managed lands ($E_{managed\ land}^{soil}$)
345 which is not necessarily reported by NGHGs. We did not try to subtract this flux from managed land emissions because we
346 assumed that, after a land use change from natural to fertilized agricultural land, background emissions decrease and become
347 very small compared to N-fertilizers induced anthropogenic emissions. In a future study, we could use for $E_{managed\ land}^{soil}$ the
348 estimate given by simulations of pre-industrial N₂O emissions from the NMIP ensemble of dynamic vegetation models with
349 carbon-nitrogen interactions (number of models; n = 7). Namely, their simulation S0 in which climate forcing is recycled
350 from 1901-1920; CO₂ is at the level of 1860, and no anthropogenic nitrogen is added to terrestrial ecosystems (Tian et al.,
351 2019).

352 Another important point to ensure a rigorous comparison between inversion and NGHGI data is whether anthropogenic
353 indirect emissions (AIE) of N₂O are reported in NGHGI reports. This is not always the case even though UNFCCC parties
354 are required to report these in their NGHGs according to the IPCC guidelines. For example, South Africa's BUR3 did not
355 report indirect N₂O emissions due to the lack of activity data. AIE arise from anthropogenic nitrogen from fertilizers leached

356 to rivers and anthropogenic nitrogen deposited from the atmosphere to soils. AIEs represent typically 20% of direct
357 anthropogenic emissions and cannot be ignored in a comparison with inversions. For Annex I countries, AIEs are
358 systematically reported, generally based on emission factors since these fluxes cannot be directly measured, and we assumed
359 that indirect emissions only occur on managed land. For non-Annex I countries, we checked manually from the original NC
360 and BUR documents if AIE was reported or not by each non-Annex I country. If AIEs were reported by a country, they were
361 used as such to compare NGHGI data with inversion results, and grouped into the agricultural sector. If they were not
362 reported, or if their values were outside plausible ranges, AIE were independently estimated by the perturbation simulation
363 of N fertilizers leaching, CO₂ and climate on rivers and lakes fluxes in the DLEM model (Yao et al., 2019), and by the
364 perturbation simulation of atmospheric nitrogen deposition on N₂O fluxes from the NMIP model ensemble (Tian et al., 2019).

365 **2.6 Grouping sectors for comparison**

366 The bottom-up NGHGIs are compiled based on activity data (statistics) following the IPCC 1996/2006 Guidelines (IPCC,
367 1997, 2006) with detailed information on subsectors. However, the top-down inversions can only distinguish between very
368 few groups of sectors at most. Thus, in this study, we aggregated NGHGI sectors into some ‘super sectors’ to make
369 inversions and inventories comparable for each GHG (**Table 2**). For CO₂, the inversions are divided into two aggregated
370 super-sectors: fossil fuel and cement CO₂ emissions, and adjusted net land flux. Inversions use a prior gridded fossil fuel
371 dataset as summarized in **Section 1.2**, thus, in this study, we compare only the net land flux between inversions and
372 inventories. To calculate the net land flux over managed lands from NGHGIs, we subtracted fossil emissions from the
373 IPCC/CRF *1. Energy* and *2. Industrial Processes* (or *2. Industrial Processes and Product Use*) sectors from the *Total GHG*
374 *emissions including LULUCF/LUCF* (or *Total national emissions and removals*) sector. For CH₄, we compare inversions
375 and inventories based on three super sectors, including *Fossil*, *Agriculture and Waste*, and *Total Anthropogenic*. To compare
376 with NGHGIs, we group the IPCC/CRF sectors of *1. Energy* and *2. Industrial Processes* (or *2. Industrial Processes and*
377 *Product Use*) by excluding Biofuel Burning (reported under *1. Energy* sector) into the super sector of *Fossil*; we group
378 sectors of *4. Agriculture* (or *3. Agriculture*) and *6. Waste* (or *5. Waste*) into the super sector of *Agriculture and Waste*; and
379 we aggregate anthropogenic flux from *Fossil* and *Agriculture and Waste* and *Biofuel Burning* into *Anthropogenic*. For N₂O,
380 we grouped the NGHGI sectors into *Anthropogenic* flux being the sum of *1. Energy* + *2. Industrial Processes* (or *2.*
381 *Industrial Processes and Product Use*) + *4. Agriculture* (or *3. Agriculture*) + *6. Waste* (or *5. Waste*) + *Anthropogenic*
382 *Indirect Emissions*.

383 **Table 2. Grouping of NGHGIs sectors into aggregated ‘super-sectors’ for comparisons with inversions.** * Biofuel burning is likely
384 not included in NGHGIs but under *1.A.4 Other Sectors* if it is reported. ** Field burning of agricultural residues is reported in Annex I
385 countries under the Agricultural sector. Note that indirect N₂O emissions are reported by Annex I countries but not systematically by non-
386 Annex I ones

Gas	Super-Sectors	Inversions	NGHGs (IPCC/CRF)
CO ₂	<i>Net Land (adjusted)</i>	<i>Flux Total - Fossil - lateral C</i>	<p>Non-Annex I (IPCC): <i>Total GHG emissions including LULUCF/LUCF - (Energy + Industrial Processes)</i></p> <p>Annex I (CRF): <i>Total national emissions and removals) - (Energy + Industrial Processes and Product Use)</i></p>
CH ₄	<i>Anthropogenic</i>	<i>Fossil + Agriculture & Waste + Biofuel Burning</i>	Energy + Industrial Processes + Agriculture + Waste + Biofuel Burning*
	<i>Fossil</i>	<i>Fossil</i>	Energy + Industrial Processes - Biofuel Burning*
	<i>Agriculture and Waste</i>	<i>Agriculture & Waste</i>	Agriculture + Waste - Field burning of agricultural residues**
N ₂ O	<i>Anthropogenic</i>	Total - pre-industrial inland waters	Agriculture + Waste direct + anthropogenic indirect emissions (AIE = anthropogenic N leached to inland waters + anthropogenic N deposited from atmosphere) + energy and industry

387 2.7 Choice of example countries for analysis

388 For the analysis, we selected 12 countries (or groups of countries) based on specific criteria for each aggregated sector.
389 Firstly, each chosen country had to possess a sufficiently large land area, as the limitations of coarse-spatial-resolution
390 inversions make it difficult to reliably estimate GHG budgets for smaller countries. Additionally, it was preferable for the
391 selected countries to have some coverage provided by the in situ global network of monitoring stations.
392 For CO₂, we focus on the land CO₂ fluxes of large fossil fuel CO₂ emitters. Although inversions do not allow to verify fossil
393 emissions in these countries as they are used as a fixed prior map of emissions, it is crucial to compare the magnitude of
394 national land CO₂ sinks with fossil fuel CO₂ emissions in those large emitters. It is important to note that fitting net fluxes to
395 changes in atmospheric CO₂ and then subtracting the prior fossil fuel (FF) fluxes can result in errors in the residual values,
396 which are typically attributed exclusively to the sum of all non-FF fluxes. Additionally, we included two large boreal
397 forested countries (Russia - RUS and Canada - CAN), two tropical countries with large forest areas (Brazil - BRA and the

398 Democratic Republic of Congo - COD), two large countries with ground-based stations (Mongolia - MNG and Kazakhstan -
399 KAZ), and two large dry Southern Hemisphere countries also with high rankings in fossil fuel CO₂ emissions (South Africa -
400 ZAF and Australia - AUS), both of which possess atmospheric stations to constrain their land CO₂ flux.

401 For CH₄, we first ranked countries (or groups of countries) based on their total anthropogenic, fossil, and agricultural
402 emissions. This study includes China (CHN), India (IND), the United States (USA), the European Union (EUR), Russia
403 (RUS), Argentina (ARG) and Indonesia (IND), all of which are among the top emitters of both fossil fuel and agricultural
404 CH₄ and possess large areas. Criteria of large land areas and the presence of atmospheric stations is crucial for in situ
405 inversions. The advantage of utilizing GOSAT in CH₄ atmospheric inversions is its ability to provide observations over
406 countries where surface in-situ data are sparse or absent, such as in the tropics. This allows us to consider countries with
407 limited or few ground-based observations. Small countries were excluded due to the coarse spatial resolution. However,
408 among the selected countries, Venezuela, with an area of 916,400 km², was chosen specifically for the analysis of CH₄
409 emissions. Despite being relatively small, Venezuela is a large producer of oil and gas, potentially allowing for inversions
410 using GOSAT satellite observations to constrain its emissions. In major oil- and gas-extracting countries that have negligible
411 agricultural and wetland emissions like Kazakhstan (KAZ), grouped in this study with Turkmenistan (TKM) into
412 KAZ&TKM; Iran (IRN); and Persian Gulf countries (GULF), fossil emissions should be easier to separate by inversions and
413 thus to be compared with NGHGs.

414 For N₂O, we selected the top 12 emitters based on the NGHGs reports. Anthropogenic N₂O emissions in most of these
415 countries are predominantly driven by the agricultural sector, which accounts for a share (including indirect emissions)
416 ranging from 6% in Venezuela (VEN) to 95% in Brazil (BRA) of their total NGHGs emissions.

417 Together, the selected countries (or groups of countries) with a different selection for each gas, account for more than 90%
418 of the global land CO₂ sink, 60% of the global anthropogenic CH₄ emissions (around 15% of fossil fuel emissions and
419 approximately 40% of agriculture and waste emissions separately), and 55% of the global anthropogenic N₂O emissions, as
420 estimated by the NGHGs.

421 **Table 3. Lists of countries or groups of countries are analyzed and displayed in the result section for each aggregated sector.**
422 Argentina (ARG), Australia (AUS), BRA (Brazil), Bangladesh (BGD), Canada (CAN), China (CHN), Columbia (COL), Democratic
423 Republic of the Congo (COD), Indonesia (IDN), India (IND), Iran (IRN), European Union (EUR), Kazakhstan (KAZ), Mexico (MEX),
424 Mongolia (MNG), Nigeria (NGA), Pakistan (PAK), Russia (RUS), South Africa (ZAF), Sudan (SDN), Thailand (THA), United States
425 (USA), Venezuela (VEN), GULF = Saudi Arabia + Oman + United Arab Emirates + Kuwait + Bahrain + Iraq + Qatar, KAZ&TKM =
426 Kazakhstan + Turkmenistan. For CH₄, acronyms underlined denotes the countries appear in both *Anthropogenic* and *Fossil* or *Agriculture*
427 *and Waste* sectors.

删除[Zhu Deng]: IND

删除[Zhu Deng]: emitter

Gas	Super Sector	Country List
-----	--------------	--------------

CO₂ *Net Land Flux* AUS, BRA, CAN, CHN, COD, EUR, IND, KAZ, MNG, RUS, USA, ZAF

CH₄ *Anthropogenic* ARG, AUS, BRA, CHN, EUR, IDN, IND, IRN, MEX, PAK, RUS, USA

Fossil CHN, EUR, GULF, IDN, IND, IRN, KAZ&TKM, MEX, NGA, RUS, USA,
VEN

Agriculture and Waste ARG, BGD, BRA, CHN, EUR, IDN, IND, MEX, PAK, RUS, THA, USA

N₂O *Anthropogenic* AUS, BRA, CHN, COD, COL, EUR, IDN, IND, MEX, SDN, USA, VEN

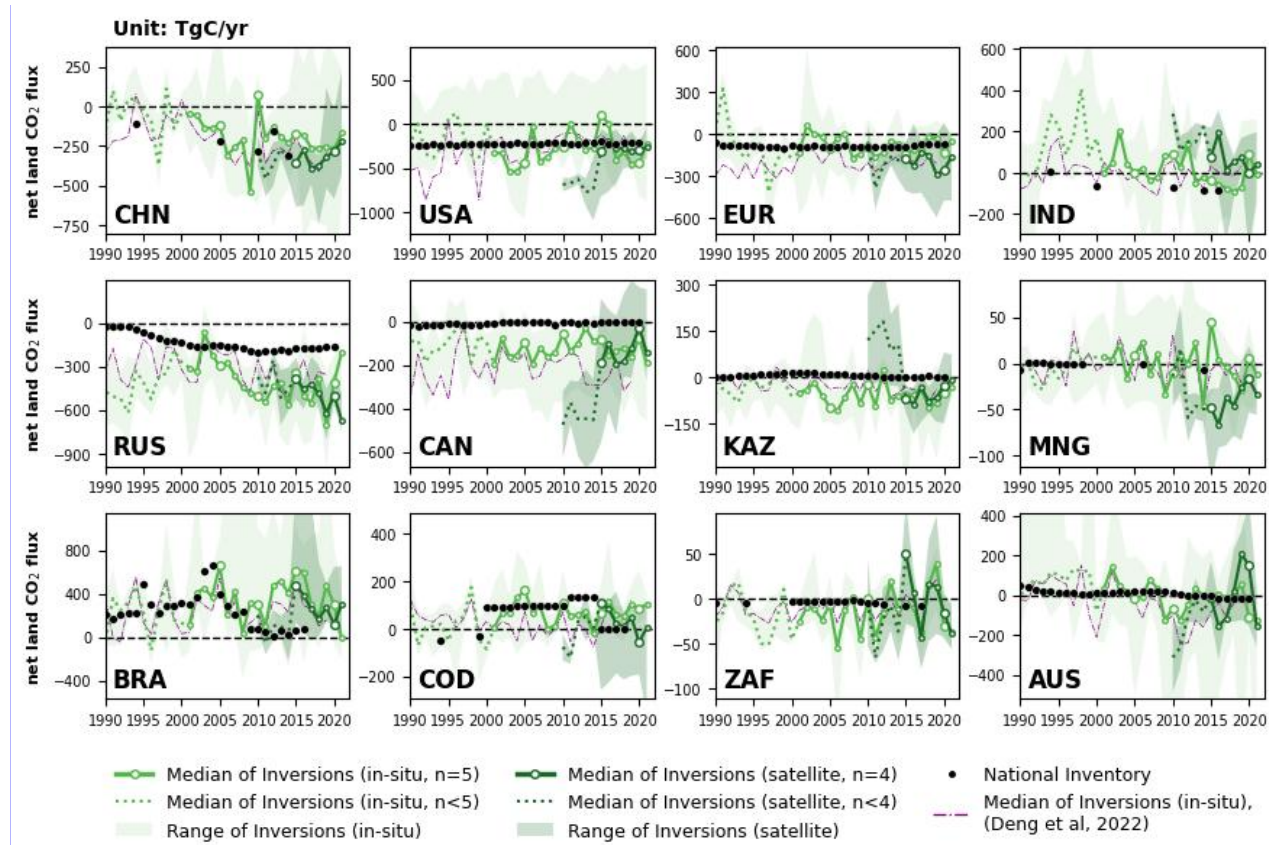
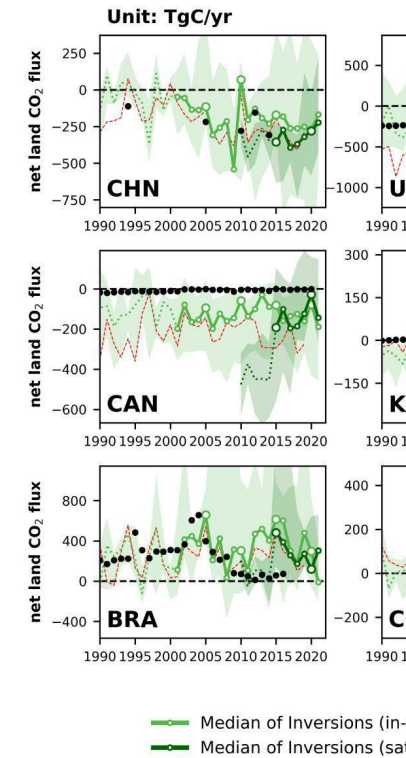


Figure 3 | Net land CO₂ fluxes (unit: TgC yr⁻¹) during 1990-2021 from China (CHN), United States (USA), European Union (EUR), Russia (RUS), Canada (CAN), Kazakhstan (KAZ), Mongolia (MNG), India (IND), Brazil (BRA), Democratic Republic of the Congo (COD), South Africa (ZAF), and Australia (AUS). By convention, CO₂ removals from the atmosphere are counted negatively, while CO₂ emissions are counted positively. The black dots denote the reported values from NGHGs. The light green color denotes the in-situ-alone CO₂ inversion (n=5) set while the dark green color denotes the set that uses satellite data (n=4). The green lines denote the median of land fluxes over managed land of CO₂ inversions, after adjustment of CO₂ fluxes from lateral transport by rivers, crop, and wood trade. When all inverse models within the inversion sets (in-situ: n=5; satellite: n=4) have available data for the same time interval, their median values are depicted as solid green lines. Otherwise, when the inversion sets have incomplete inverse models within the time interval (in-situ: n<5; satellite: n<4), their median values are represented as dashed green lines. Besides, the shading area denotes the min-max range of inversions. The purple dashed lines denote the median of inversions presented by the previous study (Deng et al., 2022).

设置格式[Zhu Deng]: 字体颜色: 自动设置



删除[Zhu Deng]:

设置格式[Zhu Deng]: 字体: 五号, 非加粗

设置格式[Zhu Deng]: 字体: 五号, 非加粗

设置格式[Zhu Deng]: 字体: 五号, 非加粗, 非上标/下标

设置格式[Zhu Deng]: 字体: 五号, 非加粗

设置格式[Zhu Deng]: 字体: 五号, 非加粗, 非上标/下标

设置格式[Zhu Deng]: 字体: 五号, 非加粗

设置格式[Zhu Deng]: 字体: 五号, 非加粗

设置格式[Zhu Deng]: 字体: 五号

设置格式[Zhu Deng]: 字体: 五号, 非上标/下标

设置格式[Zhu Deng]: 字体: 五号

设置格式[Zhu Deng]: 字体: 五号, 非上标/下标

设置格式[Zhu Deng]: 字体: 五号

设置格式[Zhu Deng]: 字体: 五号, 非上标/下标

设置格式[Zhu Deng]: 字体: 五号

443 Fig 3 presents the time series of land-to-atmosphere CO₂ fluxes for the selected countries listed in Table 2. The median of
444 inversions across the 12 countries shows significant interannual variability, reflecting the impact of climate variability on
445 terrestrial carbon fluxes and annual variations of land-use emissions.

446 The adjustments of lateral CO₂ flux generally tend to lower land carbon sinks or increase land carbon emissions, especially
447 in [China \(CHN\)](#), [United States \(USA\)](#), [European Union \(EUR\)](#), [Russia \(RUS\)](#), [Canada \(CAN\)](#), [India \(IND\)](#), and [Brazil](#)
448 [\(BRA \)](#). [In these countries, adjusting inversions by CO](#) However, even with these adjustments, in countries of temperate
449 latitudes, the median values of the five in-situ-alone inversion ensemble all indicate a net carbon sink during the 2010s, such
450 as CHN with a median sink of 180 ± 100 TgC/yr, USA (210 ± 180 TgC/yr), EUR (90 ± 50 TgC/yr), RUS (490 ± 100 TgC/yr)
451 and CAN (110 ± 40 TgC/yr). In CHN, despite only 5 reported values to UNFCCC, NGHIGs show a good agreement with
452 the inversion results, with both NGHIGs and inversions exhibiting an overall increase in carbon sink over the study period.
453 However, during 2015-2021, the median values of the satellite-based inversion ensemble show a higher carbon sink of $320 \pm$
454 60 TgC/yr than those from in-situ inversion results (220 ± 50 TgC/yr) in CHN. In IND, there are also only five reported
455 estimates from the NGHIGs. The in-situ inversion results indicate that India exhibited fluctuations between being a carbon
456 source and a carbon sink during the period of 2001-2014 (40 ± 70 TgC/yr). During 2015-2019, the in-situ inversion results in
457 IND show a median carbon sink of 65 ± 20 TgC/yr, however, the median reverted to being a carbon source of 91 TgC/yr
458 (ranging from a sink of 350 to a source of 260) in 2020. In contrast, the median values of satellite-based inversion ensemble
459 indicate a carbon source of 65 ± 60 TgC/yr during 2015-2021 in IND.

460 As Annex I countries, USA, EUR, RUS, CAN, and [Kazakhstan \(KAZ\)](#) have continuously reported annual NGHIGs since
461 1990. The NGHIGs reported values for the USA and CAN indicate a decline trend (Mann-Kendall $Z=-0.6$, $p<0.01$) of carbon
462 sinks by an annual average rate of 0.7 TgC/yr² and 0.5 TgC/yr². Like in Deng et al. 2022, we found that the carbon sink of
463 Canada's managed land is significantly larger (-125 ± 45 TgC/yr over 2001-2021 from in-situ inversions) than the NGHIGs
464 reports (5 ± 4 TgC/yr over 2001-2021). Part of this difference could be due to the fact that Canada decides in its inventory
465 not to report fire emissions as they are considered to have a natural cause. Doing so, Canada also excludes recovery sinks
466 after burning and those recovery sinks could surpass on average fire emissions, although remote sensing estimates *of post*
467 *fire biomass changes suggest that fire emissions have exceeded regrowth on average in Western*
468 *Canada and Alaska until ≈ 2010* (Wang et al., 2021). One reason for the difference may be that the NGHIG used
469 old growth curves for forests, potentially underestimating the actual forest growth. Another reason for the difference may be
470 shrubland and natural peatland carbon uptake and possibly an underestimated increase of soil carbon in the national
471 inventory. For the USA we have a good agreement between inversions (-290 ± 180 TgC/yr for in-situ over 2001-2021) and
472 the NGHIGs data (-220 ± 10 TgC/yr over 2001-2021) with the inversion showing much more interannual variability, the US
473 being a net source of carbon in the years 2011, 2015 and 2016 from the median of in-situ inversions. The lower variability in
474 the NGHIGs data reflects the 5-years averaging of C stock changes by the national forest inventory. In EUR, the new in-situ

设置格式[Zhu Deng]: 字体: 非加粗

设置格式[Zhu Deng]: 非上标/ 下标

设置格式[Zhu Deng]: 字体: 非加粗

设置格式[Zhu Deng]: 字体: 五号

设置格式[Zhu Deng]: 非上标/ 下标

设置格式[Zhu Deng]: 非突出显示

设置格式[Zhu Deng]: 非突出显示

设置格式[Zhu Deng]: 非突出显示

设置格式[Zhu Deng]: 非突出显示, 非上标/ 下标

设置格式[Zhu Deng]: 非突出显示

设置格式[Zhu Deng]: 非突出显示, 非上标/ 下标

设置格式[Zhu Deng]: 非突出显示

设置格式[Zhu Deng]: 非突出显示

设置格式[Zhu Deng]: 非突出显示

删除[Liting Hu]: t

设置格式[Zhu Deng]: 非突出显示

设置格式[Zhu Deng]: 非突出显示

设置格式[Zhu Deng]: 非突出显示

设置格式[Zhu Deng]: 非突出显示

设置格式[Zhu Deng]: 非突出显示

设置格式[Zhu Deng]: 字体: (默认) Gungshu, (中文)

Gungshu

删除[Liting Hu]: ;

475 inversion ensemble gives a lower carbon sink than the previous one (red line in Fig 3, see discussion in section 6.1), now
476 being in good agreement (-75 ± 60 TgC/yr) with NGHGs (-85 ± 10 TgC/yr) over 2001-2021. The OCO-2 satellite
477 inversions give a higher sink than in-situ inversions by -200 ± 85 Tg C/yr, possibly because the in-situ surface network does
478 not cover Eastern European countries which have a larger NEE than Western European ones, whereas OCO-2 data have a
479 more even coverage of the continent, as discussed by Winkler et al. (2023) (see their Fig. 2 showing that OCO-2 inversions
480 have a similar NEE than in-situ ones in Western Europe but a larger mean NEE uptake in Eastern Europe).

删除[Liting Hu]: OCO2

删除[Liting Hu]: OCO2

删除[Liting Hu]: OCO2

481 In contrast, the NGHGs in RUS reports a rapid trend of increasing sink by a rate of 4.6 TgC/yr² (Mann-Kendall $Z=0.69$,
482 $p<0.01$) during 1990-2020, supported by the significant strong correlation with the medians of in-situ inversion ensemble
483 ($\rho=0.7$, $p<0.01$) during 2001-2020. However, the median values for both the in-situ (480 ± 100 TgC/yr) and satellite-based
484 (450 ± 90 TgC/yr) inversion ensemble over RUS indicate larger larger land carbon sinks than those reported in the NGHGs
485 (178 ± 11 TgC/yr) during 2011-2020. For KAZ, the NGHGs suggest that managed land is a slight carbon source (6 ± 5
486 TgC/yr) during 2000-2020. However, the median values for both satellite-based and in-situ inversion ensemble indicate a
487 carbon sink of 53 ± 29 TgC/yr and 57 ± 33 TgC/yr, respectively, during 2015-2021 and 2001-2021. It is worth noting that
488 the satellite-based inversion results for USA, CAN, and KAZ all exhibit shifts in their fluxes between 2010 and 2015
489 compared to the results after 2015. This is attributed to the use of different satellite data and the number of different
490 ensembles during these periods. Before 2015, only GOSAT was available, and only 2 out of 4 systems were available. After
491 the OCO-2 record started, in September 2014, the satellite-driven inversion set only assimilated OCO-2. This indicates that
492 inversion results based on GOSAT data are not consistent at the country scale with OCO-2 inversions. As a result, we can
493 compare OCO-2 inversions with NGHGs since 2015, but not the trends from inversions using GOSAT and/or OCO-2
494 inversions since 2009.

495 In BRA, both the NGHGs reports (239 ± 166 TgC/yr during 1990-2016) and inversion results (in-situ: 350 ± 190 TgC/yr
496 during 2001-2021; satellite-based: 280 ± 120 TgC/yr during 2015-2021) indicate that the country has been a net carbon
497 source since 1990. The carbon source from managed land in Brazil increased from the late 1990s, reaching a peak around
498 2005 according to NGHGs (677 TgC/yr). This evolution is confirmed by in-situ inversions with a source peaking in 2005
499 (~ 650 TgC/yr). The net carbon source from inversions then decreased from 2005 to 2011, which is consistent with the
500 observed reduction in deforestation due to forest protection policies implemented by the Brazilian government. This is an
501 encouraging result as the inversions did not explicitly consider land use emissions in their prior assumptions, although some
502 included an estimate of carbon released by fires in their prior which is part of land-use emissions in Brazil. Since NEE is
503 defined as all land fluxes except fossil fuel emissions, NEE from all inversions nevertheless include land use emissions from
504 deforestation, degradation emissions and fire emissions including fires from deforestation, degradation and other fires. After
505 2011, inversions show a new increase in land emissions, with a peak during the 2015-2016 El Niño. There have been higher
506 average land emissions thereafter. These ongoing changes may be attributed to various factors such as the legacy effects of
507 drought leading to increased tree mortality (Aragão et al., 2018), higher wildfire emissions (Naus et al., 2022; Gatti et al.,
508 2023), carbon losses from forest degradation, and climate change-induced reductions in forest growth due to regional drying

删除[Ana Bastos]: drought

509 and warming in the southern and eastern parts of the Amazon (Gatti et al., 2021). From 2011 to 2016, the NGHGs reports
510 indicate that carbon emissions from Brazilian managed lands were stable at around 47 TgC/yr. However, the medians of in-
511 situ inversions suggest that carbon emissions rapidly increased from ~100 TgC/yr in 2011 to ~600 TgC/yr in 2016, which
512 peaked in 2015 (~610 TgC/yr). From 2016 to 2021, the medians for both in-situ and satellite inversion results show a
513 decrease in carbon emissions from 2016 to 2018 but a transient peak in 2019, a year with large fires (Gatti et al., 2023) (in-
514 situ: 480 TgC/yr; satellite: 270 TgC/yr). Then carbon emissions decreased again until 2021, which experienced wetter
515 conditions and fewer fires (Peng et al., 2022); The in-situ inversion results show a continuous decrease to -10 TgC/yr in
516 2021, while the satellite inversion results showed a persistent source carbon anomaly of 300 TgC/yr. We emphasize
517 moreover that available CO₂ observations from a network of aircraft vertical sampling (Gatti et al., 2021) were not used to
518 constrain the inverse models used here.

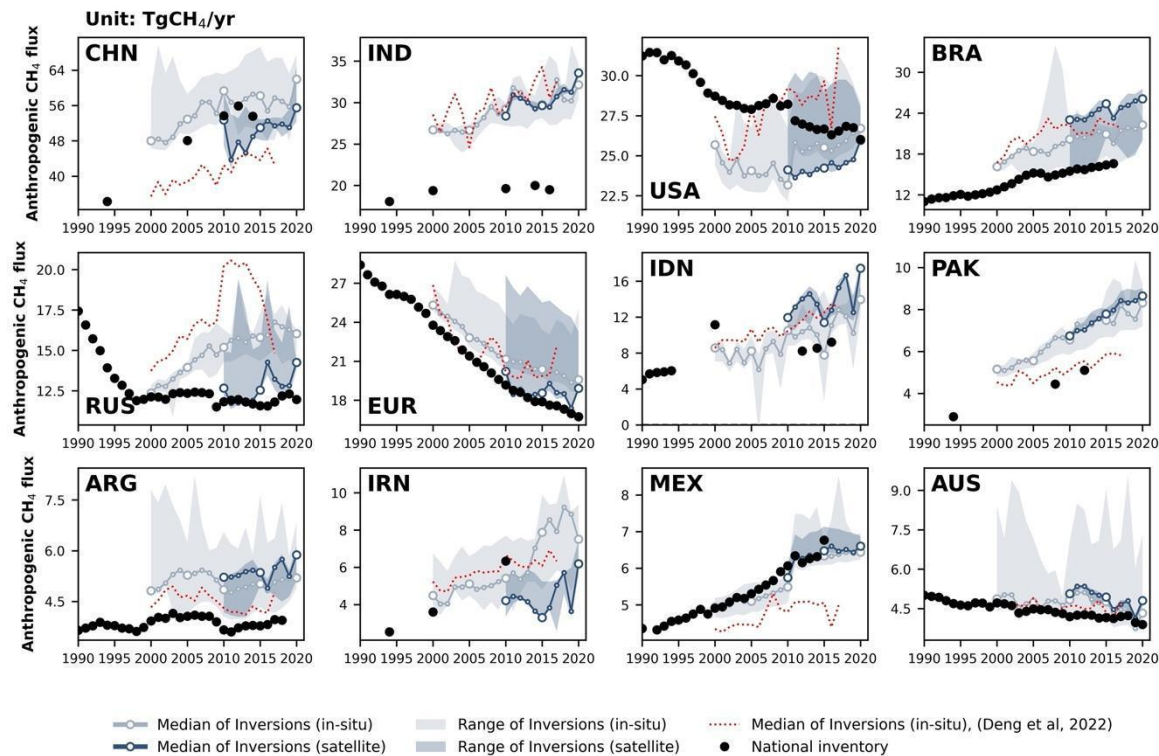
519 For [Democratic Republic of the Congo \(COD\)](#), the available NGHGs data indicates that before 2000, the country's
520 managed lands were a net carbon sink (50 TgC/yr in 1994 and 30 TgC/yr in 1999). Since 2000, the NGHGs reports
521 indicated three stages of different levels of CO₂ flux, which COD managed land was a carbon source during 2000-2010 ($95 \pm$
522 0.5 TgC/yr), a larger carbon source during 2011-2014 (135 ± 0.1 TgC/yr), and a very small sink during 2015-2018 ($-1.2 \pm$
523 0.1 TgC/yr). The medians of in-situ inversion ensemble indicate a similar annual average carbon source (70 ± 45 TgC/yr)
524 during 2001-2021 with the NGHGs, despite the few observations over Africa (Byrne et al., 2023). In the recent decade,
525 satellite inversion results from 2015 to 2021 indicate a smaller source (30 ± 55 TgC/yr) compared to the in-situ results ($85 \pm$
526 25 TgC/yr). Moreover, the satellite inversion results indicate a sink anomaly in 2020 (-60 TgC/yr) which is not found in the
527 in-situ inversions. The sink anomaly in 2020 from the satellite inversions is consistent with wetter conditions during that
528 year over COD.

529 For [South Africa \(ZAF\)](#), the NGHGs show a stable very small sink of 3 TgC/yr during 1990-2010 that doubled from 4
530 TgC/yr in 2010 to 8 TgC/yr in 2017, while the in-situ inversion results indicate large fluctuations from a carbon sink
531 (especially peaked in 2006, 2009, 2011, 2017 and 2021) to a small carbon source (e.g., in 2013, and 2018-2019). From 2015
532 to 2021, the satellite-based inversion results are consistent with the in-situ results for annual variability ($\rho=0.8$, $p<0.05$),
533 which is a good sign of the consistency between different atmospheric observing systems. During the transition to El Niño
534 conditions and drought from 2014 to 2015, however, the satellite-based inversion results indicate a switch from a carbon sink
535 to a source anomaly of 50 TgC/yr in ZAF which is not seen in the in-situ inversions.

536 In [Australia \(AUS\)](#), the NGHGs data shows a land source of carbon from 1990 to 2012, which decreased over time (from
537 48 TgC/yr in 1990 to 1 TgC/yr in 2012) and changed into a carbon sink since 2013 (that increased from a sink of 1 TgC/yr in
538 2013 to 15 TgC/yr in 2020). However, the in-situ inversions indicate fluctuations between a carbon source and a sink with an
539 annual average small sink of 10 ± 71 TgC/yr observed over the period of 2001-2021, except for 2009-2011, the medians of
540 in-situ inversions reveal a strong carbon sink of 105 ± 35 TgC/yr. Between 2010 and the strong La Niña year of 2011, the
541 medians of in-situ inversion ensemble from the previous study (Deng et al., 2022) showed an increase in carbon uptake of
542 145%. This high carbon sink persisted in 2012, which was a dryer year with maximum bushfire activity. However, in this

543 study, the medians of updated in-situ inversion ensemble indicate that there is a sink anomaly in 2011 followed by a source
544 anomaly in 2013, which appears to be more realistic. 2019 was the driest and hottest year recorded in Australia, including
545 extreme fires at the end of 2019 (Byrne et al., 2021). As a result, the medians for both in-situ and satellite inversion
546 ensemble show a carbon source anomaly in 2019, with 55 TgC/yr (ranging from a sink of 1060 to a source of 480) and 200
547 TgC/yr (ranging from a sink of 120 to a source of 320) respectively. When it comes to the wet La Niña year of 2021, the
548 medians for both in-situ and satellite inversion ensemble indicate that AUS managed land became a carbon sink of 130
549 TgC/yr (ranging from a sink of 1120 to a source of 25) and 150 TgC/yr (ranging from a sink of 260 to a source of 40).

550 Last, we give the global comparison between NGHGs and inversions, using NGHGs data compiled for all countries by
551 Grassi et al. (2023) which include Annex I countries reports, non-Annex I NC, BUR and NDCs. The river correction is the
552 only one that changes the global NEE, because the global mean of CO₂ fluxes from wood and crop products is close to zero.
553 The river-induced CO₂ uptake over land that is removed from inversion NEE is equal to the C flux transported to the ocean
554 at river mouths (0.9 GtC/yr in our estimate, close to the value of Regnier et al. 2022).The (in-situ) inversions without the
555 river correction give a global NEE sink of 1.8 GtC/yr over 2001-2020, managed land: 1.3 GtC/yr (72% of total), unmanaged
556 land: 0.5 GtC/yr (28%). The in-situ inversions with the river correction study give a global NEE sink of 0.91 GtC/yr,
557 managed land:0.51 GtC/yr (56% of total), unmanaged land 0.4 GtC/yr (44% of the total) This is an important update from
558 Deng et al. 2022 where the river CO₂ flux correction was not applied separately to managed / unmanaged lands. Because
559 managed lands have a much larger area than unmanaged ones and because of the spatial patterns of the CO₂ sinks in the
560 river correction are distributed with MODIS NPP which has low values in unmanaged lands of northern Canada and Russia,
561 the river correction reduces strongly the C storage change with respect to NEE over managed lands, and marginally in
562 unmanaged lands.. Inventory data recently compiled by Grassi et al. (2023) indicates a similar global land sink (on managed
563 land) of 0.53 GtC yr⁻¹ with gap-filled data during the same period than the inversions with our improved river correction.



566

567 **Figure 4. Total anthropogenic CH₄ fluxes for the 12 top emitters: China (CHN), India (IND), United States (USA), Brazil (BRA),**
 568 **Russia (RUS), European Union (EUR), Indonesia (IDN), Pakistan (PAK), Argentina (ARG), Iran (IRN), Mexico (MEX), and**
 569 **Australia (AUS).** The black dots denote the reported values from NGHGs. The light and dark blue lines/areas denote the median and
 570 maximum-minimum ranges of in-situ and satellite-based CH₄ inversions based on EDGARv6.0 as the prior respectively.

571 **Fig 4** presents the variations in anthropogenic CH₄ emissions for the 12 selected countries, where these emissions are
 572 summing the sectors of agriculture and waste, fossil fuels, and biofuel burning. The distribution of emissions is highly
 573 skewed even among the top 12 emitters, with the largest and most populated countries such as [China \(CHN\)](#), [India \(IND\)](#),
 574 [United States \(USA\)](#), [Brazil \(BRA\)](#), [Russia \(RUS\)](#), and [European Union \(EUR\)](#) which emits more than 10 TgCH₄/yr
 575 annually, while other countries have smaller emissions (ranging from 3 to 10 CH₄/yr) that are more challenging to quantify
 576 through inversions. During 2010-2020, CHN has the highest total anthropogenic emissions at around 50 ± 3.5 Tg CH₄/yr,
 577 followed by IND with 30 ± 1.4 Tg CH₄/yr, USA with 24 ± 0.6 Tg CH₄/yr, BRA with 24 ± 1.2 Tg CH₄/yr, EUR with 19 ± 0.7
 578 Tg CH₄/yr, [Indonesia \(IDN\)](#) with 14 ± 0.9 Tg CH₄/yr and RUS with 13 ± 0.9 Tg CH₄/yr, according to the medians of
 579 satellite-based inversion ensemble based on EDGARv6.0 as prior. The remaining countries have emissions of approximately
 580 5 Tg CH₄/yr. In general, the difference between NGHGs and inversions aligns in the same direction based on both satellite

581 and in-situ inversions. This provides some confidence for using inversions to evaluate NGHGs as the satellite observations
582 are independent from in situ networks. Overall, satellite-based inversions may be more robust across most countries due to
583 better observation coverage, except in EUR and the USA where the in-situ network is more extensive.

584 Developing countries, such as CHN, IND, BRA, IDN, [Pakistan \(PAK\)](#), [Iran \(IRN\)](#) and [Mexico \(MEX\)](#), show a rapid
585 increase in anthropogenic CH₄ emissions supported by reported values from NGHGs and results from inversions. In CHN,
586 the reported values from NGHGs (when available) generally align with the results obtained through inversions (e.g., during
587 2010-2015, NGHGs: 54 ± 1.3 Tg CH₄/yr, in-situ: 58 ± 1.2 Tg CH₄/yr, satellite-based: 48 ± 3.4 Tg CH₄/yr). During 2010-
588 2020, the median values for the in-situ and satellite-based inversion ensemble show a similar increase trend at an annual
589 growth rate of 0.28 Tg CH₄/yr² and 0.26 Tg CH₄/yr² respectively, although the medians of in-situ inversion ensemble (58 ±
590 2.0 TgCH₄/yr) were slight higher than the satellite-based ensemble (50 ± 3.5 TgCH₄/yr). However, in 2020, the medians of
591 the emission estimates for both in-situ and satellite-based inversions reveal a rapid increase by 9% and 11% compared to
592 2019 in CHN, indicating a possible surge in anthropogenic methane emissions for that year, possibly an artifact from the fact
593 that the decreased OH sink in 2020 is not well accounted for here. Indeed OH interannual variability were not prescribed to
594 all inversions, and when accounted for the OH interannual variability prescribed (based on Patra et al., 2021) was much
595 smaller than those suggested by recent studies (e.g., Peng et al., 2022). As a result overestimating the sink in the inversions
596 leads to overestimated surface emissions. The surge in emissions could also be due to spin-down, the last six month to one
597 year of inversions being less constrained by the observations, even though the inversion period covered up to June 2021.

598 In IND, PAK and MEX, there is good agreement ($r > 0.8$, $p < 0.01$) between the in-situ and satellite-based inversion ensembles
599 (respectively, 31 ± 1.2 Tg CH₄/yr and 30 ± 1.4 Tg CH₄/yr in IND, 8 ± 0.7 Tg CH₄/yr and 7 ± 0.5 Tg CH₄/yr in PAK, and 6 ±
600 0.2 Tg CH₄/yr and 6 ± 0.3 Tg CH₄/yr in MEX), while both of them present a significant increasing trend of anthropogenic
601 methane emissions in these countries (Mann-Kendall $p < 0.05$). However, when comparing to NGHGs values, the inversion
602 results in IND and PAK indicate >50% larger emissions than the values reported from the NGHGs during 2010-2020. In
603 contrast, values reported from the NGHGs (6 ± 0.2 Tg CH₄/yr) by MEX also show good agreement with the inversion
604 results.

605 In BRA, IDN and [Argentina \(ARG\)](#), the medians for in-situ and satellite-based inversion ensembles show good consistency
606 ($r = 0.8$, $p < 0.01$) in these two countries, while satellite-based inversion results are generally higher than the in-situ inversion
607 results. Specifically, in BRA, the satellite-based inversions (24 ± 1.2 Tg CH₄/yr) were 16% higher than the in-situ inversions
608 (21 ± 0.8 Tg CH₄/yr) and 52% higher than the NGHGs estimation (17 ± 0.4 Tg CH₄/yr) during 2010-2020, possibly owing
609 to difficulties for inversions to separate between natural (wetlands, inland waters) and anthropogenic sources in this country,
610 and possible flaws in the prior used for natural and anthropogenic fluxes. In IDN, NGHGs reported a significant continuous
611 upward trend at an annual average growth of 0.3 TgCH₄/yr, with a noticeable positive outlier in 2000. The medians for both
612 in-situ and satellite-based inversion ensembles also indicate an upward trend in IDN, but both of them present sudden dips in
613 anthropogenic methane emissions in 2015 and 2019 by 15~23% and 16~25%, compared to the previous year respectively. It
614 is unlikely that anthropogenic activities could contribute such large year to year variations except for different flooded areas

删除[Ana Bastos]: o

删除[Zhu Deng]: variation

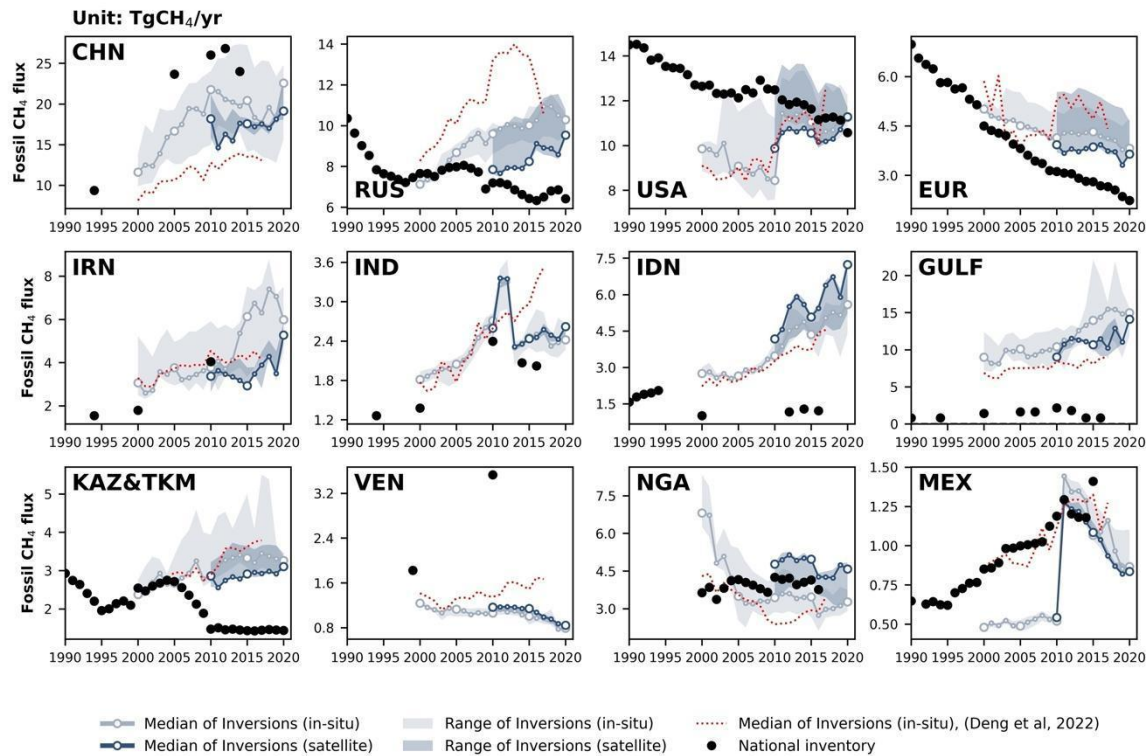
删除[Zhu Deng]: variation

615 used for rice paddies. In ARG, the satellite-based inversion results also indicate two sudden dips in 2016 and 2019, however,
616 such pattern was not found in the in-situ inversion results. A cause of year to year variations from inversions is the lack of in-
617 situ sites and variable cloud cover affecting the density of GOSAT data.

618 Regarding IRN, NGHGs only provided data for three years (1994, 2000, and 2010), making it difficult to compare with
619 inversion results. However, NGHGs show a rapid growth in anthropogenic CH₄ emissions (+9.4%/yr) during this period.
620 There are significant differences between inversion results and for IRN, with satellite inversions generally giving lower
621 emissions than in-situ inversions and different trends. Satellite inversions suggest a declining trend between 2010 and 2015,
622 followed by a fluctuating increase until 2020. In contrast, in-situ-based inversions (by any nearby measurement stations,
623 thus likely reflecting the prior trend) show a rapid rise in emissions after 2010, reaching a peak in 2018, followed by a
624 decline.

625 NGHGs for RUS indicate that anthropogenic CH₄ emissions have been reduced during the 1990s and remained stable since
626 2000 (12.0 ± 0.3 Tg CH₄/yr during 2000-2020), which is similar with the trend observed from satellite-based inversion
627 results (12.7 ± 0.9 Tg CH₄/yr during 2000-2020). However, in 2016, there was a sudden increase of emissions in satellite
628 inversion results (+14% increase from 12.5 in 2015 to 14.2 Tg CH₄/yr in 2016), followed by a gradual decline, and then a
629 new increase in 2020 (+11% increase from 12.8 Tg CH₄/yr in 2019 to 14.3 Tg CH₄/yr in 2020). This recent change was not
630 observed in the in-situ inversion results or the NGHGs.

631 For USA, [Australia \(AUS\)](#), and EUR, NGHGs reported a slow declining trend (EUR: 0.4 Tg CH₄/yr; USA: 0.2 Tg CH₄/yr;
632 AUS: -0.04 Tg CH₄/yr) in anthropogenic CH₄ emissions. In the case of the USA, inversion-derived emissions are slightly
633 lower than NGHGs (in-situ-based: 9.3% lower during 2000-2020; satellite-based: 11.4% lower during 2010-2020).
634 However, both ground-based and satellite-based inversions indicate that anthropogenic CH₄ emissions have remained
635 relatively steady since 2000, without reflecting the slow decline reported by NGHGs. In EUR, NGHGs indicate that
636 anthropogenic CH₄ emissions have been decreasing rapidly since 1990 (-1.4%/yr), consistent with the trend obtained from
637 inversion results. However, in-situ inversion emissions are on average slightly higher than NGHGs, and this difference has
638 been gradually increasing from 7.7% in the 2000s to 14.5% in the 2010s.



640

641 **Figure 5.** CH₄ emissions from the fossil fuel sector from the top 12 emitters of this sector: China (CHN), Russia (RUS), United
 642 States (USA), European Union (EUR), Iran (IRN), India (IND), Indonesia (IDN), Persian Gulf countries (GULF = Saudi Arabia +
 643 Iraq + Kuwait + Oman + United Arab Emirates + Bahrain + Qatar), Kazakhstan & Turkmenistan (KAZ&TKM), Venezuela
 644 (VEN), Nigeria (NGA), and Mexico (MEX). The black dots denote the reported value from the NGHGs. In the NGHGI data shown in
 645 Fig 5 for GULF, Saudi Arabia reported four NGHGs in 1990, 2000, 2010, and 2012, Iraq reported one in 1997, Kuwait reported three in
 646 1994, 2000, and 2016, Oman reported one in 1994, United Arab Emirates reported four in 1994, 2000, 2005 and 2014, Bahrain reported
 647 three in 1994, 2000 and 2006, and Qatar reported one in 2007. The reported values are interpolated over the study period to be summed up
 648 and plotted in the figure. For KAZ&TKM, the reported values of Turkmenistan during 2001-2003, 2005-2009, 2011-2020 are interpolated
 649 and added to annual reports from Kazakhstan, an Annex I country for which annual data are available. Other lines, colors and symbols as
 650 Fig 4.

651 **Fig 5** presents the fossil CH₄ emissions for the top 12 emitters from the fossil sector based on EDGARv6.0 as the prior. The
 652 largest emitter is [China \(CHN\)](#), mainly from the sub-sector of coal extraction, followed by [Russia \(RUS\)](#) and [United States](#)
 653 [\(USA\)](#). In CHN, the in-situ (20 ± 1.6 Tg CH₄/yr) and satellite inversions (17 ± 1.3 Tg CH₄/yr) emissions in the 2010s are
 654 24% and 35% lower than in the NGHGs (26 ± 1.5 Tg CH₄/yr), respectively. The NGHGs in CHN suggest a decrease from
 655 28 in 2012 to 24 TgCH₄/yr in 2014. However, both in-situ and satellite inversion results indicate an increasing trend since
 656 2018. In [India \(IND\)](#) and [Indonesia \(IDN\)](#), NGHGs report a decreasing trend during the study period, while inversions

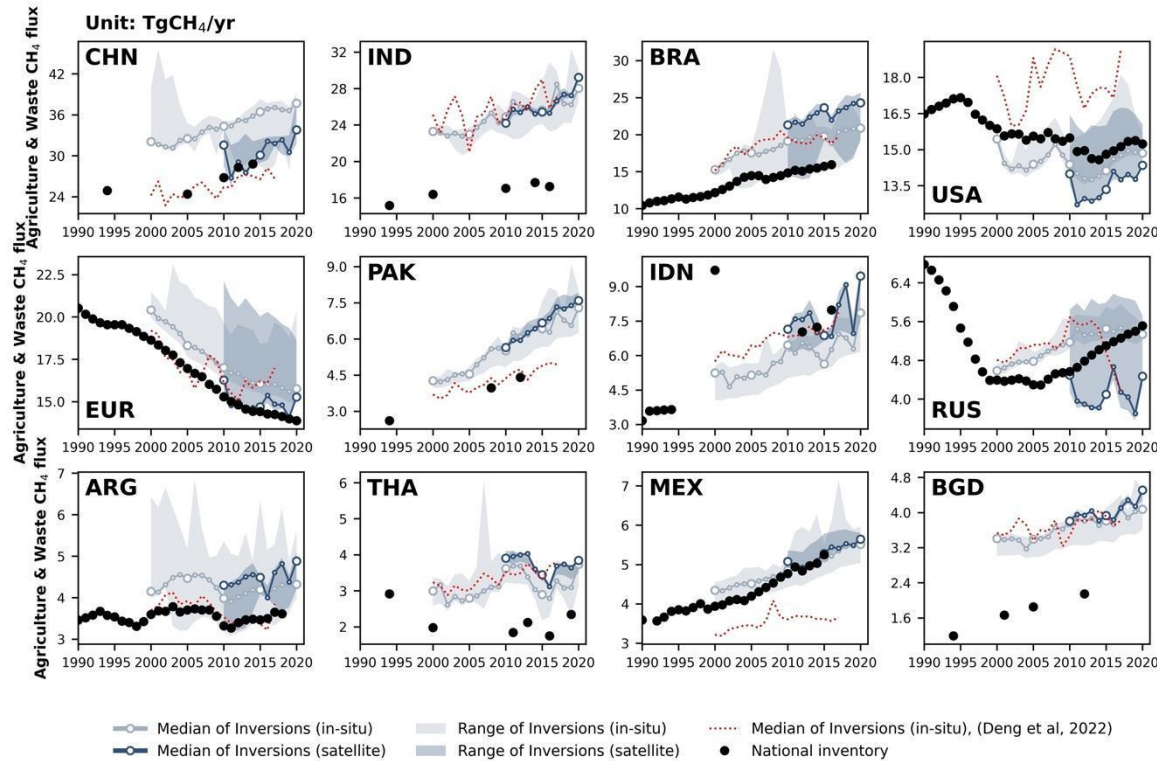
657 suggest a rapid increase in IDN and a stable value in IND after a peak in 2012. In IND, satellite inversions suggest a peak of
658 fossil CH₄ emissions during 2011-2012, which then dropped in 2013 and remained stable afterward. In IDN, both in-situ and
659 satellite inversions indicate a fluctuating trend, with a significant drop between 2015 and 2019. In RUS, both in-situ and
660 satellite inversion-based estimates of fossil fuel emissions are higher than NGHGs, and show an increasing trend, while
661 NGHGs report a decreasing trend. This discrepancy may be due to inversion problems for separating between wetland
662 emissions and gas extraction industries both located in the Yamal peninsula area, or leaks not captured in NGHGs. In USA,
663 NGHGs overall show a significant declining trend (Mann-Kendall Z=-0.8, p<0.01). In-situ inversion estimates of fossil fuel
664 emissions are 26% lower than NGHGs during 2000-2010, and remained consistent until around 2011. Nearly all in-situ
665 inversions show a jump in fossil fuel emissions in 2011. In [European Union \(EUR\)](#), both NGHGs and inversion results
666 demonstrate a consistent declining trend. However, starting from 2010, both in-situ and satellite inversions are higher than
667 NGHGs reports.

668 Major oil-producing countries in the Persian Gulf are too small compared to the model resolution to be studied individually.
669 Hence, NGHGs from the GULF countries (Saudi Arabia, Iraq, Kuwait, Oman, United Arab Emirates, Bahrain, and Qatar)
670 were grouped and show much lower emissions compared to inversion results. In the 2010s, in-situ and satellite inversions
671 estimate that emissions in GULF were 9 times and 8 times higher than the estimates reported in NGHGs, respectively. This
672 huge under-reporting of emissions in GULF could be partly attributed to the omission of ultra-emitters in NGHGs. [The
673 ultra-emitters defined by Lauvaux et al. \(2022\) are namely all short-duration leaks from oil and gas facilities \(e.g., wells,
674 compressors\) with an individual emission >20 t CH₄ h⁻¹, each event lasting generally less than one day. Such leaks are often
675 random occurrences and difficult to quantify, which is why most countries do not account for these significant and episodic
676 events in the national inventories.](#) Indeed, recent studies by Lauvaux et al. (2022) have identified more ultra-emitters and
677 larger emission budgets from ultra-emitters in Qatar, Kuwait, and Iraq. In KAZ&TKM, grouped together because of their
678 rather small individual areas, both in-situ (3.3 ± 0.2 Tg CH₄/yr) and satellite (2.9 ± 0.1 Tg CH₄/yr) inversions estimate
679 emissions to be 2 times higher than NGHGs (1.5 ± 0.1 Tg CH₄/yr) in the 2010s. Similarly, KAZ is located downwind of
680 TKM, which has a high share of ultra-emitters. The global inversions operating at a coarse resolution may misallocate
681 emissions from TKM to KAZ. It is worth noting that KAZ has two in-situ stations for CH₄ measurements, whereas the
682 GULF countries lack in-situ station networks. On the other hand, the GOSAT satellite provides a dense sampling of
683 atmospheric column CH₄ in the Persian Gulf region due to frequent cloud-free conditions. Therefore, GOSAT inversions can
684 be considered more accurate than in-situ inversions for [Iran \(IRN\)](#), GULF countries, and [Kazakhstan & Turkmenistan
685 \(KAZ&TKM\)](#). Additionally, it is important to note that GOSAT inversions generally give lower emissions than in-situ
686 inversions in those countries. [Venezuela \(VEN\)](#) is a rare case where NGHGs report much higher CH₄ emissions than
687 inversions. While the uncertainty of GOSAT inversions (model spread) has decreased compared to the results reported by
688 Deng et al. 2022, the gap between inversions and NGHGs has increased. In 2010, NGHGs reports of fossil CH₄ emissions
689 in VEN were 298% higher than GOSAT inversions and 326% than in-situ inversions. We do not have a clear explanation
690 for this large difference, except that VEN has strongly decreased oil and gas extraction due to sanctions curbing its crude

691 production from 2.65 mb/d in 2015 to 0.57 mb/d in 2020 (OPEC, 2023), which may not be reflected in their NGHGs. In
 692 [Nigeria \(NGA\)](#) and [Mexico \(MEX\)](#), NGHGs estimates fall between the median of in-situ and satellite inversions during
 693 2010-2020. However, in MEX, the in-situ inversion was 50% lower than NGHGs in the 2000s and showed a sudden large
 694 increase in 2010.

删除[Liting Hu]: NGA
 删除[Liting Hu]:

695 **4.3 Agriculture and waste CH₄ emissions**

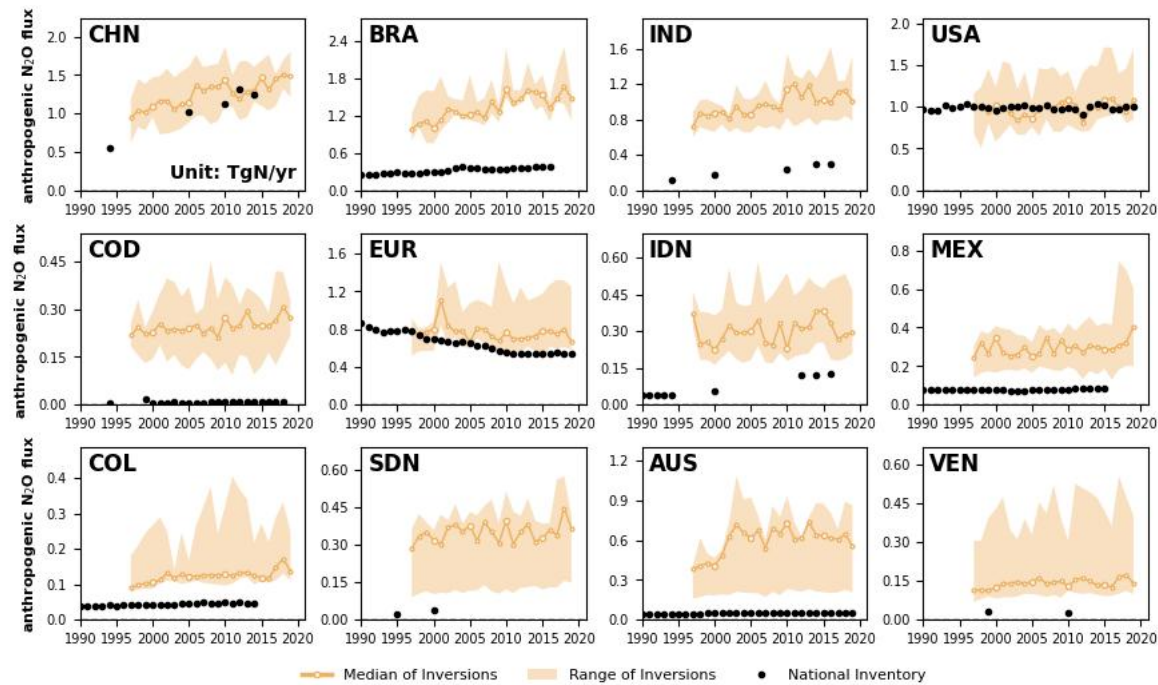


696 **Figure 6. CH₄ emissions from agriculture and waste for the 12 largest emitters in this sector, China (CHN), India (IND), Brazil**
 697 **(BRA), United States (USA), European Union (EUR), Pakistan (PAK), Indonesia (IDN), Russia (RUS), Argentina (ARG),**
 698 **Thailand (THA), Mexico (MEX), and Bangladesh (BGD).** The black dots denote the reported estimates from NGHGs. Other lines,
 699 colors, and symbols as Fig 4.

701 **Fig 6** presents CH₄ emissions of the Agriculture and Waste sector for the top 12 emitters of this sector. In all countries
 702 except for the [United States \(USA\)](#) and [Russia \(RUS\)](#), the values reported by NGHGs are systematically lower than the
 703 inversion results. The results from the previous ensemble of in-situ inversions (red dotted line) are consistent with those of
 704 the inversions used in this study except in the USA where previous inversions are 3.2 TgCH₄/yr higher, in RUS where they
 705

706 | show a drop after 2015 although they remain in the range from the new satellite and in-situ inversions, and in [Mexico \(MEX\)](#)
707 | where they are systematically lower by 1.6 TgCH₄/yr.

708 | In [China \(CHN \)](#), the most recent NGHGI reports in 2012 and 2014 estimate agriculture and waste emissions at 28 Tg
709 | CH₄/yr, which is close to satellite inversions (28 ± 1 TgCH₄/yr) but 22.4% lower than the median in-situ inversions (35 ±
710 | 0.5 TgCH₄/yr) and closer to their minimum value. The trend in agricultural and waste emissions is consistent between
711 | inversions and NGHGI reports for CHN. In [India \(IND \)](#), inversions consistently show higher emissions than NGHGI reports by
712 | approximately 50% and indicate an increasing trend during 2000-2020, whereas the NGHGI last communication being for
713 | 2016, it does not allow us to give a recent trend. According to the national inventory of IND, enteric fermentation is the
714 | primary source of CH₄ emissions in the agriculture and waste sector, contributing 61% of emissions, with rice cultivation
715 | accounting for 20% and waste contributing 16%. A similar pattern is observed in [Bangladesh \(BGD \)](#), where agricultural
716 | emissions are dominated by rice production (48% in 2012) and enteric fermentation (42% in 2012). Satellite and in-situ
717 | inversions estimate emissions in BGD are nearly double than those reported by NGHGI reports during 2001 and 2012, the last
718 | communication. The significant discrepancies between inversions and NGHGI reports in IND and BGD may be attributed to
719 | potential underestimation of livestock or waste CH₄ emissions by NGHGI reports. NGHGI reports utilized the Tier 1 method and
720 | associated emission factors from the 2006 IPCC Guidelines for National Greenhouse Gas Inventories (IPCC, 2006).
721 | However, a recent study (Chang et al., 2021) found that estimates using revised Tier 1 or Tier 2 methods from the 2019
722 | Refinement to the 2006 IPCC Guidelines for National Greenhouse Gas Inventories (IPCC, 2019) give livestock emissions
723 | 48%-60% and 42%-61% higher for IND and BGD by 2010, respectively, compared to Tier 1 IPCC (2006) methods, which
724 | would bring bottom up emissions closer to inversions. In [Brazil \(BRA \)](#), both satellite and in-situ inversions consistently
725 | estimate larger emissions than the NGHGI reports by 34% and 29%, respectively, and show a consistent increasing trend over their
726 | study periods. In the USA, the medians of satellite and in-situ inversions are slightly lower than those of NGHGI reports, but they
727 | exhibit a similar trend throughout the study period. The trend of inversions is comparable to the one of the NGHGI reports in BRA
728 | during their period of overlap, although there is no NGHGI communication later than 2016. In [Argentina \(ARG \)](#), [Pakistan](#)
729 | [\(PAK \)](#) and [Thailand \(THA \)](#), the medians of in-situ inversions show good consistency with satellite inversion results.
730 | Nevertheless, in-situ inversion emissions in the 2010s are, on average, 47% higher in PAK, 20% higher in ARG, and 64%
731 | higher in THA compared to the NGHGI reports. In [European Union \(EUR \)](#), emissions from agriculture and waste were
732 | reported to have significantly decreased over time in the NGHGI data, mainly from solid waste disposal (Petrescu et al.,
733 | 2021), a trend that is captured by inversions and is close to the one of the NGHGI reports over the study period. In contrast,
734 | emissions from agriculture and waste in RUS are reported to have a positive trend after 2010 by the NGHGI, with in-situ
735 | inversions producing a consistent trend from 2000 to 2014 but a sharp decrease thereafter, while satellite inversions are
736 | producing stable emissions, albeit lower than the NGHGI reports and in-situ inversions after 2010.



738

739 **Figure 7. Anthropogenic N₂O fluxes of the top 12 emitters: China (CHN), Brazil (BRA), India (IND), United States (USA),**
 740 **Democratic Republic of the Congo (COD), European Union (EUA), Indonesia (IDN), Mexico (MEX), Colombia (COL), Sudan**
 741 **(SDN), Australia (AUS), and Venezuela (VEN).** The black dots denote the anthropogenic emissions from the UNFCCC national
 742 greenhouse gas inventories. The thick orange lines and the light orange areas denote the median and the maximum-minimum ranges of
 743 anthropogenic fluxes respectively among all N₂O inversions. We restricted our analysis to data starting from 1997 because it was the year
 744 when data from the all four inversion models are available.

745

746 We present the 12 countries/regions with the largest anthropogenic N₂O emissions in the world (**Fig 7**), which in total
 747 contribute approximately 55% of global anthropogenic N₂O emissions. The estimates from both NGHGs and inversions in
 748 [China \(CHN\)](#), [United States \(USA\)](#), and [European Union \(EUR\)](#) demonstrate a relatively close match between NGHGs and
 749 inversions (in-situ only). These three large emitting countries/regions exhibit different trends in their anthropogenic N₂O
 750 emissions. In CHN, both NGHGs and inversions indicate an increasing trend in anthropogenic N₂O emissions. In the USA,
 751 anthropogenic N₂O emissions seem to have reached a state of relative stability, with NGHGs and inversion results showing
 752 similar mean values and lack of trends. In EUR, both NGHGs and inversions show a declining trend in anthropogenic N₂O
 753 emissions, but from 2010 to 2020, the NGHGs estimates are lower (20%) than the median values derived from inversion
 754 models, that is, the negative trend from inversions is less pronounced than the one of NGHGs. Most other selected countries
 755 display higher anthropogenic N₂O emissions from inversions than from NGHGs (i.e., [Brazil \(BRA\)](#), [India \(IND\)](#),

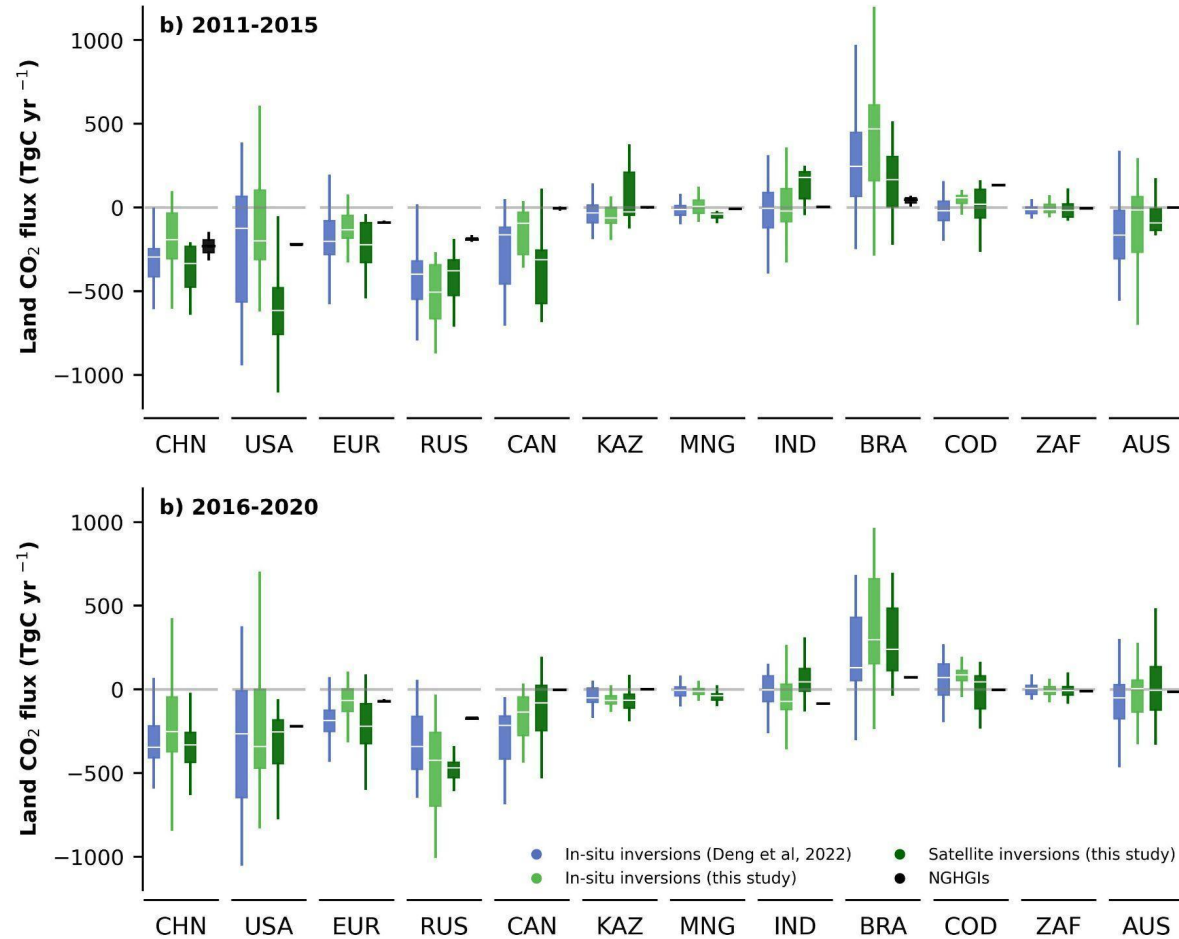
设置格式[Zhu Deng]: 字体: 小五, 非突出显示

756 | [Democratic Republic of the Congo \(COD\)](#), [Indonesia \(IDN\)](#), [Mexico \(MEX\)](#), [Colombia \(COL\)](#), [Sudan \(SDN\)](#), [Venezuela](#)
757 | [\(VEN\)](#)). These discrepancies in anthropogenic N₂O emissions are possibly attributable to factors that have been analyzed in
758 | our previous study (Deng et al., 2022). Firstly, nearly all these non-Annex 1 countries utilize Tier 1 emission factors (EFs),
759 | which may underestimate emissions, when soil and climate dependence [are](#), taken into account (Cui et al., 2021). This has
760 | been noted in previous studies (Philibert et al., 2013; Shcherbak et al., 2014; Wang et al., 2020). Furthermore, the observed
761 | concave response of cropland soil emissions as a function of added N fertilizers may also contribute to underestimated
762 | emissions in NGHGs, as the relationship is non-linear and higher than the linear relation used by NGHGs in Tier 1
763 | approaches (Zhou et al., 2015). In an improved reporting framework, EFs should also account for both natural and
764 | anthropogenic components, as they cannot be distinguished through field measurements, from which EFs are derived.
765 | However, in practice, EFs are mostly based on measurements made in temperate climates and soils from established
766 | croplands with few "background" emissions. Consequently, there could be a systematic underestimation of default IPCC EFs
767 | from tropical climates and for recently established agricultural lands, for which the IPCC EFs also have a huge uncertainty of
768 | up to ±75%–100%. Another factor that might contribute to the discrepancy is the omission of emissions from reactive
769 | nitrogen contained in organic fertilizers (manure), for which NGHGs do not provide specific details for non-Annex 1
770 | reports. Lastly, anthropogenic indirect emissions (AIEs) from atmospheric nitrogen deposition and leaching of human-
771 | induced nitrogen additions to aquifers and inland waters are reported by Annex 1 countries using simple emission factors,
772 | but non-Annex 1 countries do not consistently report AIE. However, in [Australia \(AUS\)](#), the gap between inversions and
773 | NGHGs is even expanded compared to our previous study. We do acknowledge that the density of the N₂O in-situ network
774 | in tropical countries and around AUS is so low that inversions most likely are attracted to their priors. The use of a lower
775 | prior could thus also be consistent with scarce atmospheric observations, and we have only a low confidence on N₂O
776 | inversion results for tropical countries and AUS.

删除[Liting Hu]:

删除[Liting Hu]: n

删除[Liting Hu]: is



779 **Figure 8.** Net CO₂ land fluxes during the period of a) 2011-2015; and b) 2016-2020 in China (CHN), United States (USA),
 780 European Union (EUR), Russia (RUS), Canada (CAN), Kazakhstan (KAZ), Mongolia (MNG), India (IND), Brazil (BRA),
 781 Democratic Republic of the Congo (COD), South Africa (ZAF), and Australia (AUS). Blue boxes denote the in-situ inversion results
 782 from Deng et al. (2022) processed from Global Carbon Budget 2020 (Friedlingstein et al., 2020). Light green boxes denote the in-situ
 783 inversion results processed in this study, while dark green boxes denote the satellite inversion results. Black boxes denote the NGHGs
 784 reported values. The white lines in the boxes denote the medians of the land CO₂ fluxes. Note that the inversion results here have been
 785

786 adjusted by the lateral flux before the comparison. [Additionally, we extend the comparison with national land use change emissions from](#)
787 [global bookkeeping models in Fig S4.](#)

788 In this section, we compare four different estimates of land CO₂ fluxes during the period 2010-2020 (**Fig 8**), including: 1)
789 medians of in-situ inversion results from our previous study (Deng et al., 2022), 2) medians of in-situ and 3) satellite-based
790 inversion results processed in this study based on the Global Carbon Budget 2022 (Friedlingstein et al., 2022), and 4)
791 NGHGs. This enables a comparison of the median and range of our in-situ inversion results (n=5) with those from previous
792 study (n=6), and assesses the performance differences between satellite-based (n=4) and in-situ inversion models. To ensure
793 a fair comparison and avoid anomalies in the satellite-based inversion results during 2010-2015 when some of these
794 inversions used GOSAT after 2010 and then OCO-2 after 2015, we separate the analysis into two periods: 2011-2015 and
795 2016-2020.

796 The variations of yearly land CO₂ fluxes span a comparable range between the current and previous in-situ inversion
797 ensembles, indicating that consistency of the inversion results, but the uncertainty within the new in-situ inversion ensemble
798 was not improved. However, examining the median values, results from the new in-situ inversion ensemble may be closer to
799 NGHGs in most countries (such as [China \(CHN\)](#), [United States \(USA\)](#), [European Union \(EUR\)](#), [Canada \(CAN\)](#),
800 [Kazakhstan \(KAZ\)](#), [India \(IND\)](#)). This suggests that the new in-situ inversion ensemble used in this study has partially
801 narrowed down the gaps between inversion results and NGHGs compared to the previous one. However, in [Russia \(RUS\)](#)
802 and [Brazil \(BRA\)](#), the difference between the median of in-situ inversion ensembles and NGHGs has enlarged. For example,
803 in RUS, median the new in-situ inversion ensemble indicate a larger carbon sink than those from Deng et al. (2022), while
804 the difference between median of in-situ inversions and NGHGs increases 51% during 2011-2015 (from 208 TgC/yr to 314
805 TgC/yr) and 49% during 2016-2020 (from 168 TgC/yr to 249 TgC/yr). Conversely, in BRA, median of the new in-situ
806 inversion ensemble indicate a larger carbon source, while the difference increases over 100% during 2011-2015 (from 200
807 TgC/yr to 423 TgC/yr) and nearly 300% during 2016-2020 (from 56 TgC/yr to 223 TgC/yr).

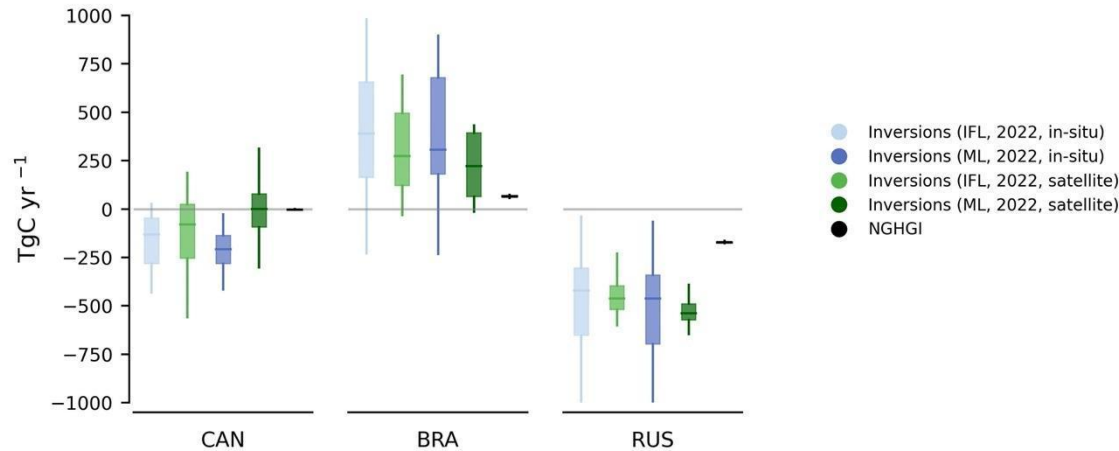
808 As for the inversion ensemble used in this study, in most countries, the variations of yearly land CO₂ fluxes also span a
809 similar range between satellite-based inversion ensemble and in-situ inversion ensemble. However, in the cases of USA,
810 RUS, CHN and BRA, the spread of satellite-based inversion results are narrower than those of in-situ inversion results,
811 indicating a better consistency among available satellite-based inversion models, at least when similar satellite data are
812 assimilated. In addition, in most cases, smaller difference [s](#) were found between the median of inversion results and the
813 NGHGs. For countries with dense surface monitoring networks such as in the USA and EUR, the satellite-based inversion
814 results show good agreement in-situ inversion results. However, for countries with sparse station coverage like [Kazakhstan](#)
815 [\(KAZ\)](#) and [Mongolia \(MNG\)](#), satellite-based inversion results could provide more reliable estimates due to more extensive
816 spatial sampling from satellites, although the medians of satellite-based inversion results indicate larger carbon sinks and
817 larger differences compared with NGHGs (than for in-situ inversion results). In USA and CAN, the difference during 2011-
818 2015 (only GOSAT period) between in-situ and satellite-based inversion ensembles [is](#) larger than that during 2016-2020
819 ([OCO-2](#) period). This can be attributed to the use of different satellite data during these periods and different numbers of

删除[Liting Hu]: are

删除[Liting Hu]: OCO2

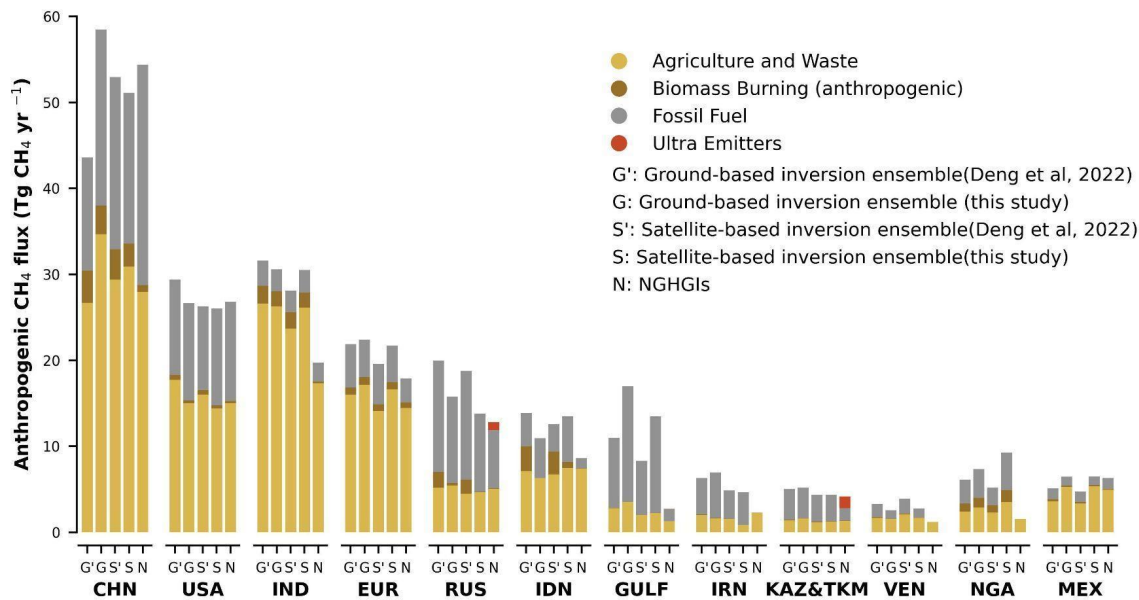
820 ensemble members. Before 2015, only GOSAT was available, and only 2 out of 4 systems. The inversion of OCO-2 data
 821 starting in 2014 result in a better alignment among OCO-2 ACOS v10 inversions, indicating the in-situ and satellite
 822 evaluations were similar (Byrne et al., 2023).

823 **6.2 Adjustment of the national managed land masks to separate the net land CO₂ flux estimates**



824 **Figure 9. Net CO₂ land fluxes during the period of 2015-2020 in Canada (CAN), Brazil (BRA), and Russia (RUS).** ‘IFL’ stands for
 825 using the intact forest landscape data as a mask for non-managed land to extract land CO₂ flux from managed land and ‘ML’ indicates the
 826 adjusted mask used by Grassi et al. (2023) to extract land CO₂ flux from managed land. The ‘in-situ’ stands for inversion results using in-
 827 situ observations, and ‘satellite’ represents inversions using satellite observations. Note that the inversion results here have been adjusted by
 828 the lateral flux before the comparison.
 829

830 Following the method proposed by Grassi et al. (2023), we updated in this study the managed land mask for [Canada \(CAN\)](#)
 831 and [Brazil \(BRA\)](#) by using maps of managed land derived from NGHGI, and for [Russia \(RUS\)](#) by adjusting tree-cover
 832 threshold in the tree cover map from Hansen et al. (2013) to match the average area of managed land per Oblast (province)
 833 that is used for the NGHGIs. Thus, the new mask is now more consistent with the definition of managed land in the
 834 NGHGIs for these three countries, so that can further analyze the impacts of different definitions of managed land masks to
 835 separate the managed land CO₂ fluxes in inversions (**Fig 9**). Generally, in Russia (RUS) and Canada (CAN), the managed
 836 land CO₂ fluxes extracted from the new mask are closer to NGHGIs than those separated by the previous mask used by
 837 Deng et al. 2022. In addition, in Brazil (BRA), adjusting the national managed land mask resulted in greater land carbon
 838 emissions, increasing the gap with NGHGIs. However, the improvement of the managed land mask in this study is still not
 839 able to explain all the existing discrepancy between inversion estimates and NGHGIs, in which the sources and reasons for
 840 these differences and uncertainties still need further analysis. We also observe in **Fig. 9** that the impact of our new managed
 841 land mask compared to the previous one, is qualitatively similar whether it is applied to in-situ inversions or satellite
 842 inversions gridded flux fields.

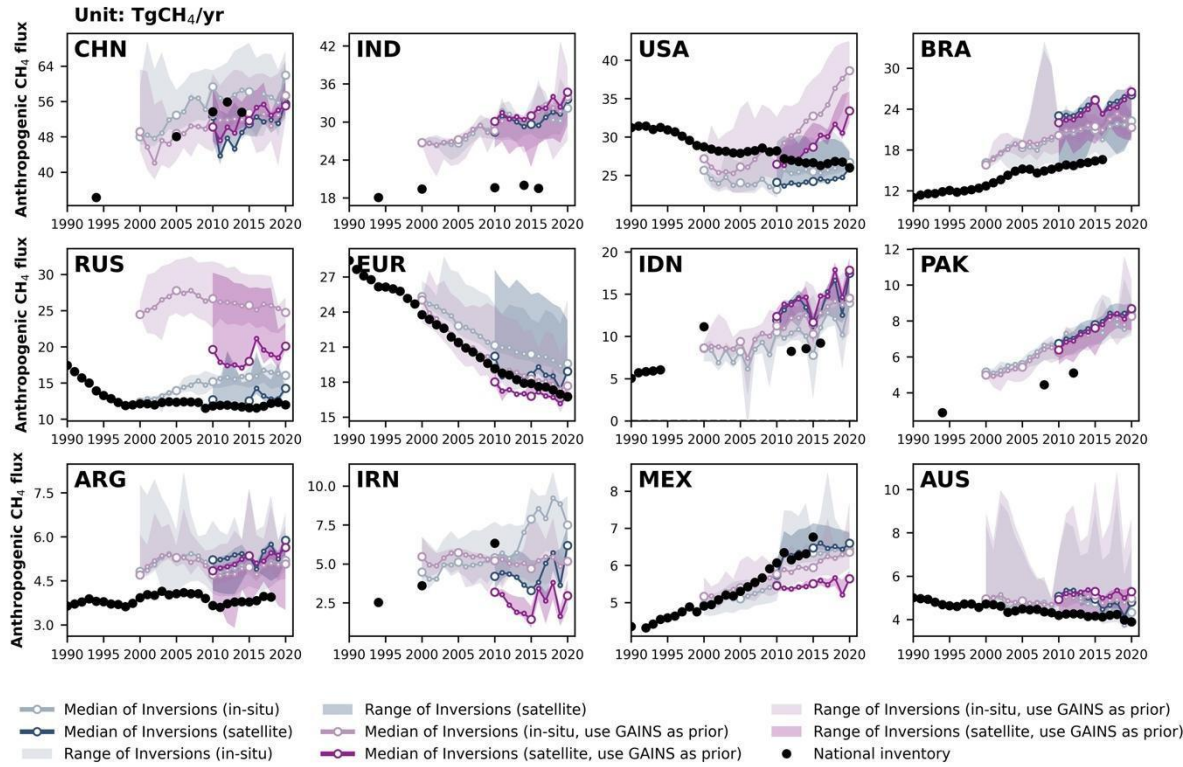


844
845 **Figure 10. Annual average of anthropogenic CH₄ emissions from in-situ (G) and satellite (S) inversions and national greenhouse**
846 **gas inventories (N) during the period of 2010-2020. G' and S' denote the anthropogenic CH₄ flux from the in-situ and satellite inversion**
847 **ensembles in the previous study (Deng et al., 2022) respectively, while G and S denote the fluxes from the in-situ and satellite inversion**
848 **ensembles used in this study. N denotes the estimates from NGHGs. Grey, yellow, and brown bars represent the CH₄ fluxes from the**
849 **sectors of fossil fuel combustion, agriculture and waste, and biomass burning respectively. On top of NGHGI emissions, emissions from**
850 **ultra-emitters (red) are added to NGHGI estimates (diagnosed from S5P-TROPOMI measurements for the period 2019–2020; Lauvaux et**
851 **al., 2022).**

852 In our previous study, we found that satellite inversion models appear to have a better agreement with NGHGs than in-situ
853 stations based inversion models, and on the other hand, that differences between inversion models and NGHGs in large oil-
854 and gas-producing countries suggest an underestimation of national reports, possibly due to the omission of ultra-emitting
855 sources by NGHGs. With the new inversion ensemble in this study, we confirm those results (**Fig 10**). In countries such as
856 [China \(CHN\)](#), [India \(IND\)](#), and [Russia \(RUS\)](#), the updated inversion model set provides estimates that are closer to NGHGs,
857 but differences still exist, and the reasons for these differences are not the same. For example, differences in anthropogenic
858 methane emissions in IND are mainly due to differences in agricultural and waste methane flux with the new inversion
859 ensemble used in this study. In RUS, the updated inversion ensemble shows lower fossil fuel emissions, reducing the
860 differences with NGHGs for this sector, but higher agricultural and waste emissions than in Deng et al. (2022). Nevertheless,
861 the updated fossil fuel emission flux is still higher than the NGHGs estimate for RUS. The remaining differences may be
862 attributed to ultra-emitting sources or underestimated emission factors for some components of the oil and gas extraction and
863 distribution industry in RUS. Conversely, in GULF ([GULF = Saudi Arabia + Iraq + Kuwait + Oman + United Arab Emirates](#)

864 + Bahrain + Qatar), the new inversion model ensemble consistently reflects higher fossil fuel emission fluxes than NGHGs
 865 like in our previous study, and expands the difference in estimates of artificial methane flux between inversion models and
 866 NGHGs, possibly indicating more methane leakage.

867 **6.4 Influence of the prior used in CH₄ inversions**



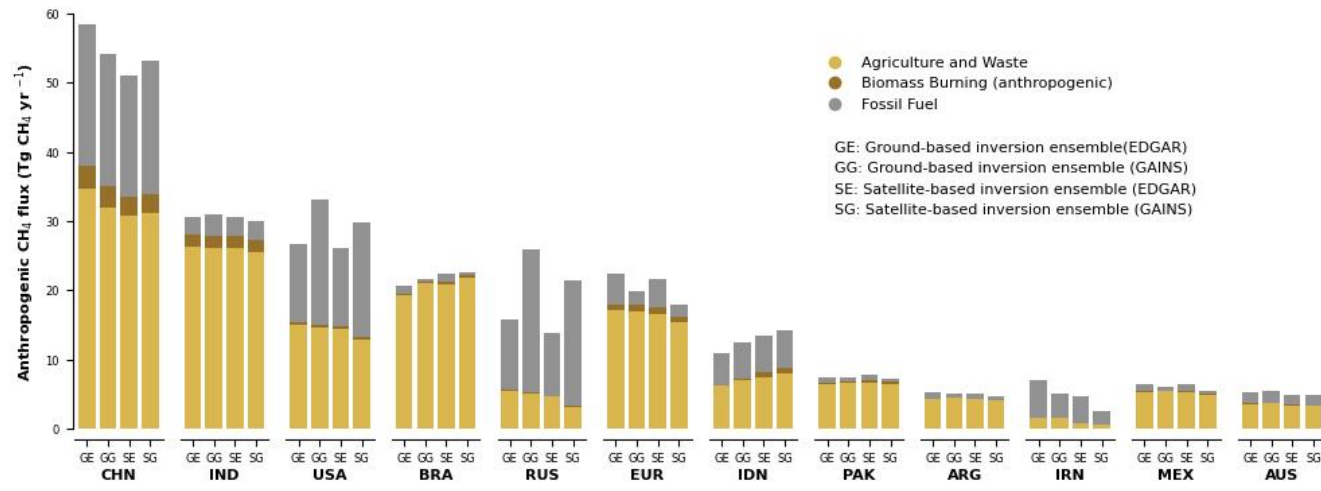
868
 869 **Figure 11. Total anthropogenic CH₄ fluxes for the 12 top emitters: China (CHN), India (IND), United States (USA), Brazil (BRA),**
 870 **Russia (RUS), European Union (EUR), Indonesia (IDN), Pakistan (PAK), Argentina (ARG), Iran (IRN), Mexico (MEX), and**
 871 **Australia (AUS).** The black dots denote the reported values from NGHGs. The light blue lines/areas denote the median and maximum-
 872 minimum ranges of in-situ CH₄ inversions based on EDGARv6.0 as the prior and the dark blue ones of satellite inversions, respectively.
 873 The light purple lines/areas denote the median and maximum-minimum ranges of in-situ CH₄ inversions based on GAINS (Höglund-
 874 Isaksson et al., 2020) as the prior and the dark purple ones of satellite inversions, respectively.

875
 876 The use of different priors can also influence the inversion results of the data. **Fig 11** presents the sets of inversion results
 877 using EDGAR (blue) and GAINS (purple) as priors. In most countries, the median values of the two inversion result sets are
 878 similar. However, in countries such as [Russia \(RUS\)](#), [United States \(USA\)](#), [Iran \(IRN\)](#), [Mexico \(MEX\)](#), significant
 879 differences are observed between the two inversion result sets, which may primarily stem from the differences in the

删除[Zhu Deng]:

880 inversion results for fossil CH₄ emissions (**Fig 1 2**). In RUS and USA, the inversion results using GAINS as priors are
 881 consistently higher than those using EDGAR as priors. In RUS, the satellite inversion results using GAINS as priors are
 882 higher by 45% during 2010-2020, and the ground-based inversion results are higher by 75% during 2000-2020. In the case
 883 of the USA, the inversion results using GAINS as priors exhibit a completely different trend compared to the ones obtained
 884 using NGHGs and EDGAR as priors. The inversion results using GAINS as priors, both from satellite and ground-based
 885 measurements, show a rapid growth trend by increasing 24% from 2010 to 2020. In IRN and MEX, the inversion results
 886 using GAINS as priors are lower than those using EDGAR as priors. For IRN, the differences between satellite inversion
 887 results using different priors are not significant, and the trends are similar. However, the ground-based inversion results are
 888 very close between 2000-2013, but after 2013, a steep increase is observed in the ground-based inversion results using
 889 GAINS as priors. On the other hand, in MEX, the ground-based inversion results are similar, but the satellite inversion
 890 results using GAINS as priors are relatively lower by 14% averagely. Such discrepancies may arise from differences in
 891 inventory methodologies and the resulting estimations. As shown in Supplementary Figure S1 in Tibrewal et al. (2024),
 892 similar discrepancies were found between the two inventories in these countries, which reports a higher estimation from
 893 GAINS in RUS and USA compared to EDGAR during 2011-2020, and a lower estimation in IRN. As noted in Tibrewal et al.
 894 (2024), EDGAR is based on various versions of National Inventory Reports (NIR) that utilize different combinations of
 895 emission factors from the IPCC, while GAINS employs an independent estimation approach. This highlights the critical role
 896 of prior data selection in determining the accuracy of CH₄ emission estimates.

删除[Zhu Deng]: SI



设置格式[Zhu Deng]: 图案: 清除(自动设置)

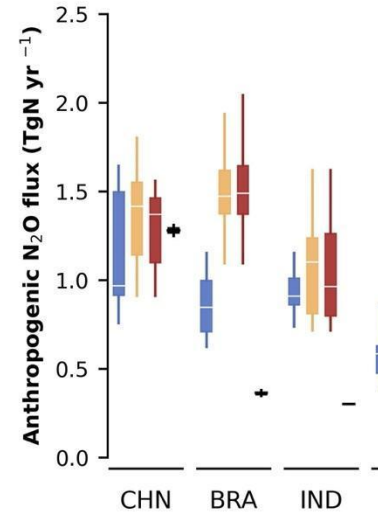
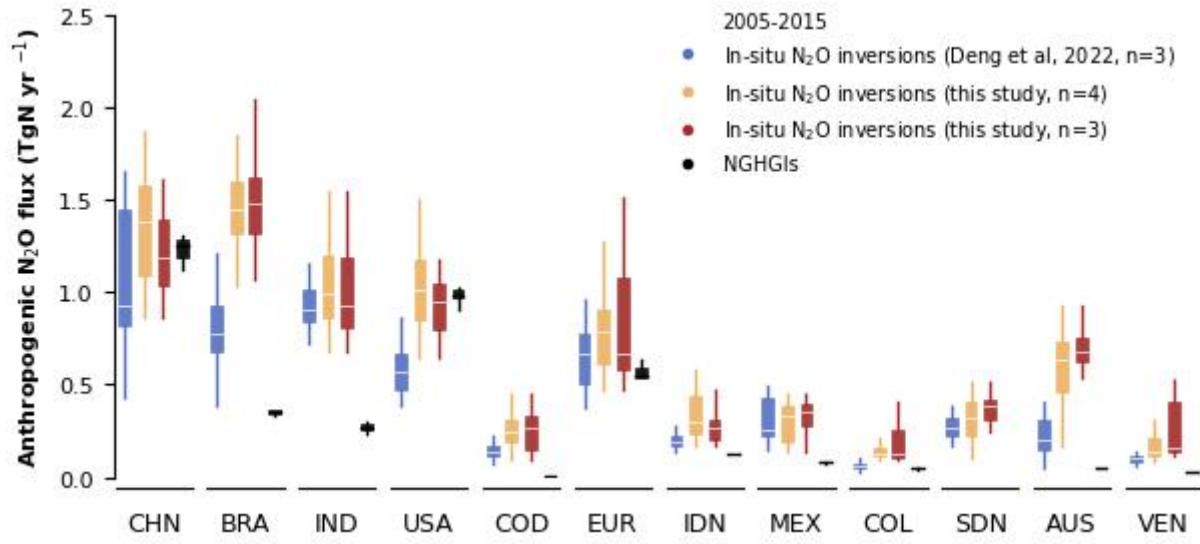
设置格式[Zhu Deng]: 图案: 清除(自动设置)

897

898

设置格式[Zhu Deng]: 图案: 清除(自动设置)

设置格式[Zhu Deng]: 图案: 清除(自动设置)



900 **Figure 13.** Anthropogenic N₂O fluxes during the period of 2005-2015, in China (CHN), Brazil (BRA), India (IND), United States
 901 (USA), Democratic Republic of the Congo (COD), European Union (EUR), Indonesia (IDN), Mexico (MEX), Colombia (COL),
 902 SDN (Sudan), Australia (AUS), and Venezuela (VEN). Blue boxes denote the in-situ inversion results from Deng et al. 2022 processed
 903 from Global Carbon Budget 2020 (Friedlingstein et al., 2020). Dark yellow boxes denote the inversion results processed in this study.
 904 Black boxes denote the NGHGs reported values.

905
 906
 907 The updated N₂O inversion results show systematically higher anthropogenic emissions than the previous N₂O inversion
 908 results (Deng et al., 2022), resulting in larger discrepancies between N₂O inversion results and NGHGs in most countries in
 909 Fig 13. Countries such as Brazil (BRA), Democratic Republic of the Congo (COD), Indonesia (IDN), Colombia (COL),
 910 Sudan (SDN), Australia (AUS), and Venezuela (VEN) exhibit significant differences. United States (USA), in the case of the
 911 USA, the median of the updated N₂O inversion results is very close to NGHGs. The median of the N₂O inversion results
 912 from Deng et al. (2022) was 42% lower than the NGHGs between 2005 and 2015, whereas the median of the updated
 913 inversion models is only 4% lower. This demonstrates improved consistency in the updated inversion system results for the
 914 USA. Additionally, in countries such as India (IND), IDN, COL, COD, Sudan (SDN), and VEN, our N₂O inversion results
 915 have a larger distribution compared to the previous study, indicating that the new N₂O inversion ensemble (n=4) has less
 916 consistency in these countries compared to the previous ensemble (n=3).

917 **Conclusions**

918 This study reconciles the gap between atmospheric inversions and UNFCCC NGHGs for each of the three greenhouse gases,
 919 based on the post-processing framework we proposed in our previous study (Deng et al., 2022). We update inversion results

- 删除[Zhu Deng]:
- 删除[Zhu Deng]: 2
- 删除[Zhu Deng]: 10
- 删除[Zhu Deng]: 2020
- 删除[Zhu Deng]: Overall, t
- 删除[Zhu Deng]: are
- 删除[Zhu Deng]: in most countries
- 删除[Liting Hu]: USA
- 删除[Zhu Deng]: (
- 删除[Zhu Deng]: 3
- 删除[Zhu Deng]: 2
- 删除[Zhu Deng]: our
- 删除[Zhu Deng]: I
- 删除[Zhu Deng]: addition, in
- 删除[Liting Hu]:
- 删除[Liting Hu]:

920 and NGHGIs datasets to present the most-up-to-date discrepancies between these two estimates. For CO₂, we updated the
921 inversion results up to 2021, added a new inversion ensemble including inversions based on satellite observations, and
922 applied a new mask of national managed land based on NGHGI reports in Russia, Brazil and Canada. For CH₄, we compared
923 NGHGIs and CH₄ inversion results up to 2020 by splitting the anthropogenic fluxes from inversions by aggregating prior
924 estimates from each sector or by removing fluxes of natural processes and discussed the uncertainties by using different
925 priors in CH₄ inversions. For N₂O, we updated the inversion results up to 2019 and included the MIROC4-ACTM N₂O
926 inversion, also separated the fluxes from managed land by using the same method on CO₂.

927 In the case of CO₂, we updated the managed land mask for Canada, Brazil, and Russia based on maps derived from NGHGIs
928 and adjusted tree-cover thresholds. The analysis of different managed land mask definitions shows that the new mask, which
929 is more consistent with the definition of managed land in the NGHGIs for these countries, improves the agreement between
930 managed land CO₂ fluxes and NGHGIs in Russia and Canada. However, in Brazil, the new mask increases the gap between
931 the estimated land carbon emissions and NGHGIs. Further analysis is needed to understand the sources and reasons for
932 discrepancies and uncertainties between inversion estimates and NGHGIs. Thus, we still recommend that countries should
933 report their managed land in a spatially explicit manner to enable a better evaluation of national emission reports using
934 inversions (and other observation-based approaches), and countries should also follow the recommendations of the IPCC
935 2006 Guidelines encouraging countries to use atmospheric data as an independent check on their national reports (IPCC
936 2006, 2019). Three additional satellite-based inversion results have been introduced for comparison with the in-situ inversion
937 results and NGHGIs. In some countries, the satellite-based inversions demonstrate better consistency with NGHGIs
938 compared to the in-situ inversion models.

939 For CH₄, despite the large spread of inversions, both in-situ and GOSAT inversions show systematic differences with
940 NGHGIs. We also found that Kazakhstan and Turkmenistan in Central Asia and the Gulf countries in the Middle East,
941 characterized by oil- and gas-producing industries, report much less CH₄ emissions than atmospheric inversions estimates.
942 While in this region, there are few ground stations, and inversions depend on their prior fluxes, the fact that GOSAT and in-
943 situ based inversions point to NGHGI emissions being underestimated suggests areas for future research to constrain the
944 emissions of these countries. We recommend here to develop regional campaigns (such as those performed in Alvarez et al.
945 (2018)), to refine emission factors, and to track regional oil, gas and coal basins emissions and ultra-emitter site-level
946 emissions using new tools (such as moderate and high-resolution satellite imagery).

947 For N₂O, the prevalence of large tropical natural sources, being outside the responsibility of countries if they are located on
948 unmanaged lands, has been overlooked before. For example, nearly half of the forests in Brazil are unmanaged according to
949 its national inventory report. We did not solve this problem, but highlighted it and proposed a new method to remove natural
950 emissions from inversion total emissions. As many non-Annex I countries, which will have to produce inventories for the
951 global stocktake are tropical countries with a very active nitrogen cycle and large natural N₂O emissions, a decoupling will
952 exist between targeted emissions reductions and the observed growth rate of N₂O: it may hamper the eventual effectiveness
953 of mitigation policies, that are directly reflected in the UNFCCC NGHGIs reports, especially for this greenhouse gas. It is

删除[Zhu Deng]: In this study,

954 fair to say that the uncertainty from the spread of different inversions is large enough that inversions cannot ‘falsify’ N₂O
955 NGHGs in most instances. Nevertheless, for CH₄ in countries around the Persian Gulf and Central Asia, and to some extent
956 in Russia, and for N₂O in tropical countries, Mexico and Australia, we found that NGHGs emissions are significantly lower
957 than inversions, which suggests that activity data or emission factors may need to be re-evaluated. Despite their large spread,
958 inversions have the advantage of providing fluxes that are consistent with the accurately observed growth rates of each
959 greenhouse gas in the atmosphere. The uncertainty of inversions is mainly a systematic bias due to internal settings or to the
960 choice of a transport model. It does not mean that inversions cannot be used for monitoring interannual variability and trends
961 of fluxes, in response to mitigation efforts, since most of their bias should have a small temporal component.
962 The study of global inversions at the country scale rather than at the traditional subcontinent scale (e.g. the “Transcom3
963 regions” of Gurney et al. (2002)) obviously pushes inversions close to the limit of their domain of validity, even in the case
964 of large countries. The densification of observation networks and systems, especially from space, increases the observational
965 information available at all spatial scales and gradually makes it possible to study smaller countries and reduce uncertainties
966 of inversion results. This densification must be accompanied by a corresponding increase in the horizontal resolution of
967 inversion systems (both the transport model and the control vector to be optimized). Note that the spatial resolution of most
968 inverse models such as those contributing to the global carbon/methane/nitrous oxide budget is larger than 1 degree (see
969 Table A4 in Friedlingstein et al. (2022), Table S6 in Saunio et al. (2020), and Table 1 in Tian et al. (2023)). They will likely
970 soon have to go below one degree on a global scale to remain competitive for this type of study, despite the high
971 computational challenge posed by the atmospheric inversion of long-lived tracers.

972 **Data availability**

973 Processed GHG (CO₂, CH₄, and N₂O) data from inverse models and UNFCCC NGHGs are available at
974 <https://doi.org/10.5281/zenodo.13887128> (Deng et al., 2024).

975 This dataset contains 5 data files:

- 976 - The file *Inversions_CO2_y2022.csv* includes the NEE CO₂ flux from managed lands for the nine CO₂ inverse
977 models. It includes 8 fields: years (from 1960 to 2021), country, value (unit: TgC/yr), sector ("land": without the
978 adjustment of lateral C flux; "land_cor": with later C flux adjustment), source, gas, observation ("in-situ": in-situ-
979 based; "satellite": satellite-based), version ("CO₂_ML_v2022" only).
- 980 - The file *Inversions_CH4_y2022.csv* includes CH₄ flux from anthropogenic sources for the six CH₄ inverse models.
981 It includes 8 fields: years (from 2000 to 2020), country, value (unit: TgCH₄/yr), sector ("agr": agriculture and
982 waste; "fos": fossil fuel; "ant": anthropogenic=agrw+fos), source, gas, observation ("in-situ": in-situ-based;
983 "satellite": satellite-based), version ("CH₄_2022_V1": use EDGAR as priors; "CH₄_2022_V2": use GAINS as
984 priors).

删除[Zhu Deng]: <https://doi.org/10.5281/zenodo.10841716>

- 985 - The file *Inversions_N2O_v2022.csv* includes the anthropogenic N2O flux from managed lands for the four N2O
986 inverse models. It includes 8 fields: years (from 1995 to 2020), country, value (unit: TgN2O/yr), sector ("ant" only,
987 for anthropogenic), source, gas, observation ("in-situ" only, for in-situ-based), version ("N2O_ML_v2022" only).
988 - The file *lateral_CO2_v2022.csv* includes the national lateral C flux from river and trade.
989 - The file *NGHGs_v2022.csv* includes the national inventory data collected from UNFCCC NGHGs (unit: Gg/yr)

990 Author contribution

991 PC, FC, MS, RLT, and ZD designed and coordinated the study. PC, MS, RLT, and FC designed the framework of
992 atmosphere inversion data processing. ZD, PC, LH, MS, RLT, and FC performed the post-processing and analysis and wrote
993 the paper. ZD, LH, and TW compiled the national greenhouse gas inventories. MS, RLT, HT, and FC gathered the global
994 atmosphere inversion datasets of CO₂, CH₄, and N₂O. GG contributed the managed land mask of Brazil and Canada. FC
995 processed the atmosphere inversion data with masks of managed lands and country boundaries. AT, SM, RJ, YN, BZ, JT,
996 DB and AS contribute the unpublished CH₄ inversion data. All authors contributed to the full text.

997 Competing interests

998 At least one of the (co-)authors is a member of the editorial board of Earth System Science Data.

999 Acknowledgements

1000 The authors are very grateful to the atmosphere inversion model developers, Chris Wilson, Christian Rödenbeck, Kelley
1001 Wells, Liesbeth Florentie, Naveen Chandra, Peter Bergamaschi, Prabir Patra, and Yi Yin, for the availability of their global
1002 CO₂, CH₄, and N₂O inversion data and acknowledge many other data providers (measurements, models, inventories,
1003 atmospheric inversions, hybrid products, etc.) that are directly or indirectly used in this synthesis. [The PyVAR-CAMS N2O
1004 modelling results were funded through the Copernicus Atmospheric Monitoring Service, implemented by ECMWF on behalf
1005 of the European Commission and were generated using computing resources from LSCE. Rona Thompson would also like to
1006 acknowledge the support of Frederic Chevallier in providing the PyVAR-CAMS N2O inversion results.](#)

删除[Zhu Deng]: Aki Tsuruta, Arjo Segers, Bo Zheng,

删除[Shamil]: Misa Ishizawa,

删除[Shamil]: Shamil Maksyutov,

删除[Zhu Deng]: , and Yosuke Niwa

1007 References

1008 Aragão, L. E. O. C., Anderson, L. O., Fonseca, M. G., Rosan, T. M., Vedovato, L. B., Wagner, F. H., Silva, C. V. J., Silva Junior, C. H. L.,
1009 Arai, E., Aguiar, A. P., Barlow, J., Berenguer, E., Deeter, M. N., Domingues, L. G., Gatti, L., Gloor, M., Malhi, Y., Marengo, J. A.,
1010 Miller, J. B., Phillips, O. L., and Saatchi, S.: 21st Century drought-related fires counteract the decline of Amazon deforestation

1011 carbon emissions, *Nat. Commun.*, 9, 536, 2018.

1012 Berchet, A., Sollum, E., Thompson, R. L., Pison, I., Thanwerdas, J., Broquet, G., Chevallier, F., Aalto, T., Berchet, A., Bergamaschi, P.,
1013 Brunner, D., Engelen, R., Fortems-Cheiney, A., Gerbig, C., Groot Zwaaftink, C. D., Haussaire, J.-M., Henne, S., Houweling, S.,
1014 Karstens, U., Kutsch, W. L., Lujikx, I. T., Monteil, G., Palmer, P. I., van Peet, J. C. A., Peters, W., Peylin, P., Potier, E., Rödenbeck,
1015 C., Saunio, M., Scholze, M., Tsuruta, A., and Zhao, Y.: The Community Inversion Framework v1.0: a unified system for
1016 atmospheric inversion studies, *Geoscientific Model Development*, 14, 5331–5354, 2021.

1017 Byrne, B., Liu, J., Lee, M., Yin, Y., Bowman, K. W., Miyazaki, K., Norton, A. J., Joiner, J., Pollard, D. F., Griffith, D. W. T., Velazco, V.
1018 A., N. M. Deutscher, Jones, N. B., and Paton-Walsh, C.: The carbon cycle of southeast Australia during 2019–2020: Drought, fires,
1019 and subsequent recovery, *AGU Advances*, 2, <https://doi.org/10.1029/2021av000469>, 2021.

1020 Byrne, B., Baker, D. F., Basu, S., Bertolacci, M., Bowman, K. W., Carroll, D., Chatterjee, A., Chevallier, F., Ciais, P., Cressie, N., Crisp,
1021 D., Crowell, S., Deng, F., Deng, Z., Deutscher, Nicholas M, Dubey, M. K., Feng, S., García, O. E., Griffith, D. W. T., Herkommer,
1022 B., Hu, L., Jacobson, A. R., Janardanan, R., Jeong, S., Johnson, M. S., Jones, D. B. A., Kivi, R., Liu, J., Liu, Z., Maksyutov, S.,
1023 Miller, J. B., Miller, S. M., Morino, I., Notholt, J., Oda, T., O'Dell, C. W., Oh, Y.-S., Ohyama, H., Patra, P. K., Peiro, H., Petri, C.,
1024 Philip, S., Pollard, D. F., Poulter, B., Remaud, M., Schuh, A., Sha, M. K., Shiomi, K., Strong, K., Sweeney, C., Té, Y., Tian, H.,
1025 Velazco, V. A., Vrekoussis, M., Warneke, T., Worden, J. R., Wunch, D., Yao, Y., Yun, J., Zammit-Mangion, A., and Zeng, N.:
1026 National CO₂ budgets (2015–2020) inferred from atmospheric CO₂ observations in support of the global stocktake, *Earth System
1027 Science Data*, 15, 963–1004, 2023.

1028 Chandra, N., Patra, P. K., Bisht, J. S. H., Ito, A., Umezawa, T., Saigusa, N., Morimoto, S., Aoki, S., Janssens-Maenhout, G., Fujita, R.,
1029 Takigawa, M., Watanabe, S., Saitoh, N., and Canadell, J. G.: Emissions from the Oil and Gas Sectors, Coal Mining and Ruminant
1030 Farming Drive Methane Growth over the Past Three Decades, *Journal of the Meteorological Society of Japan. Ser. II*, 99, 309–337,
1031 2021.

1032 Chang, J., Ciais, P., Gasser, T., Smith, P., Herrero, M., Havlík, P., Obersteiner, M., Guenet, B., Goll, D. S., Li, W., Naipal, V., Peng, S.,
1033 Qiu, C., Tian, H., Viovy, N., Yue, C., and Zhu, D.: Climate warming from managed grasslands cancels the cooling effect of carbon
1034 sinks in sparsely grazed and natural grasslands, *Nat. Commun.*, 12, 118, 2021.

1035 Chevallier, F.: Fluxes of carbon dioxide from managed ecosystems estimated by national inventories compared to atmospheric inverse
1036 modeling, *Geophys. Res. Lett.*, 48, <https://doi.org/10.1029/2021gl093565>, 2021.

1037 Chevallier, F., Fisher, M., Peylin, P., Serrar, S., Bousquet, P., Bréon, F.-M., Chédin, A., and Ciais, P.: Inferring CO₂sources and sinks
1038 from satellite observations: Method and application to TOVS data, *J. Geophys. Res.*, 110, <https://doi.org/10.1029/2005jd006390>,

1039 2005.

1040 Ciais, P., Yao, Y., Gasser, T., Baccini, A., Wang, Y., Lauerwald, R., Peng, S., Bastos, A., Li, W., Raymond, P. A., Canadell, J. G., Peters,
1041 G. P., Andres, R. J., Chang, J., Yue, C., Dolman, A. J., Haverd, V., Hartmann, J., Laruelle, G., Konings, A. G., King, A. W., Liu, Y.,
1042 Luysaert, S., Maignan, F., Patra, P. K., Peregon, A., Regnier, P., Pongratz, J., Poulter, B., Shvidenko, A., Valentini, R., Wang, R.,
1043 Broquet, G., Yin, Y., Zscheischler, J., Guenet, B., Goll, D. S., Ballantyne, A.-P., Yang, H., Qiu, C., and Zhu, D.: Empirical estimates
1044 of regional carbon budgets imply reduced global soil heterotrophic respiration, *Natl Sci Rev*, 8, nwaal45, 2021.

1045 Cui, X., Zhou, F., Ciais, P., Davidson, E. A., Tubiello, F. N., Niu, X., Ju, X., Canadell, J. G., Bouwman, A. F., Jackson, R. B., Mueller, N.
1046 D., Zheng, X., Kanter, D. R., Tian, H., Adalibieke, W., Bo, Y., Wang, Q., Zhan, X., and Zhu, D.: Global mapping of crop-specific
1047 emission factors highlights hotspots of nitrous oxide mitigation, *Nat Food*, 2, 886–893, 2021.

1048 Deng, Z., Ciais, P., Tzompa-Sosa, Z. A., Saunio, M., Qiu, C., Tan, C., Sun, T., Ke, P., Cui, Y., Tanaka, K., Lin, X., Thompson, R. L.,
1049 Tian, H., Yao, Y., Huang, Y., Lauerwald, R., Jain, A. K., Xu, X., Bastos, A., Sitch, S., Palmer, P. I., Lauvaux, T., d’Aspremont, A.,
1050 Giron, C., Benoit, A., Poulter, B., Chang, J., Petrescu, A. M. R., Davis, S. J., Liu, Z., Grassi, G., Albergel, C., Tubiello, F. N.,
1051 Perugini, L., Peters, W., and Chevallier, F.: Comparing national greenhouse gas budgets reported in UNFCCC inventories against
1052 atmospheric inversions, *Earth Syst. Sci. Data*, 14, 1639–1675, 2022.

1053 Deng, Z., Ciais, P., Hu, L., Wang, T., Martinez, A., Saunio, M., Thompson, R., and Chevallier, F.: Global greenhouse gas reconciliation
1054 2022, 2024. <https://doi.org/10.5281/zenodo.13887128>

1055 Feng, L., Palmer, P. I., Parker, R. J., N. M. Deutscher, Feist, D. G., Kivi, R., Morino, I., and Sussmann, R.: Estimates of European uptake
1056 of CO₂ inferred from GOSAT XCO₂ retrievals: sensitivity to measurement bias inside and outside Europe, *Atmos. Chem. Phys.*, 16,
1057 1289–1302, 2016.

1058 [Flammini, A., Adzmir, H., Karl, K., and Tubiello, F. N.: Quantifying greenhouse gas emissions from wood fuel use by households, *Earth*](#)
1059 [Syst. Sci. Data](#), 15, 2179–2187, <https://doi.org/10.5194/essd-15-2179-2023>, 2023.

1060 Friedlingstein, P., O’Sullivan, M., Jones, M. W., Andrew, R. M., Hauck, J., Olsen, A., Peters, G. P., Peters, W., Pongratz, J., Sitch, S., Le
1061 Quéré, C., Canadell, J. G., Ciais, P., Jackson, R. B., Alin, S., Aragão, L. E. O. C., Arneeth, A., Arora, V., Bates, N. R., Becker, M.,
1062 Benoit-Cattin, A., Bittig, H. C., Bopp, L., Bultan, S., Chandra, N., Chevallier, F., Chini, L. P., Evans, W., Florentie, L., Forster, P. M.,
1063 Gasser, T., Gehlen, M., Gilfillan, D., Gkritzalis, T., Gregor, L., Gruber, N., Harris, I., Hartung, K., Haverd, V., Houghton, R. A.,
1064 Ilyina, T., Jain, A. K., Joetzjer, E., Kadono, K., Kato, E., Kitidis, V., Korsbakken, J. I., Landschützer, P., Lefèvre, N., Lenton, A.,
1065 Lienert, S., Liu, Z., Lombardozzi, D., Marland, G., Metzl, N., Munro, D. R., Nabel, J. E. M. S., Nakaoka, S.-I., Niwa, Y., O’Brien, K.,
1066 Ono, T., Palmer, P. I., Pierrot, D., Poulter, B., Resplandy, L., Robertson, E., Rödenbeck, C., Schwinger, J., Séférian, R., Skjelvan, I.,

1067 Smith, A. J. P., Sutton, A. J., Tanhua, T., Tans, P. P., Tian, H., Tilbrook, B., van der Werf, G., Vuichard, N., Walker, A. P.,
1068 Wanninkhof, R., Watson, A. J., Willis, D., Wiltshire, A. J., Yuan, W., Yue, X., and Zaehle, S.: Global carbon budget 2020, *Earth*
1069 *Syst. Sci. Data*, 12, 3269–3340, 2020.

1070 Friedlingstein, P., O’Sullivan, M., Jones, M. W., Andrew, R. M., Gregor, L., Hauck, J., Le Quéré, C., Lujckx, I. T., Olsen, A., Peters, G. P.,
1071 Peters, W., Pongratz, J., Schwingshackl, C., Sitch, S., Canadell, J. G., Ciais, P., Jackson, R. B., Alin, S. R., Alkama, R., Arneeth, A.,
1072 Arora, V. K., Bates, N. R., Becker, M., Bellouin, N., Bittig, H. C., Bopp, L., Chevallier, F., Chini, L. P., Cronin, M., Evans, W., Falk,
1073 S., Feely, R. A., Gasser, T., Gehlen, M., Gkritzalis, T., Gloege, L., Grassi, G., Gruber, N., Gürses, Ö., Harris, I., Hefner, M.,
1074 Houghton, R. A., Hurtt, G. C., Iida, Y., Ilyina, T., Jain, A. K., Jersild, A., Kadono, K., Kato, E., Kennedy, D., Klein Goldewijk, K.,
1075 Knauer, J., Korsbakken, J. I., Landschützer, P., Lefèvre, N., Lindsay, K., Liu, J., Liu, Z., Marland, G., Mayot, N., McGrath, M. J.,
1076 Metzl, N., Monacci, N. M., Munro, D. R., Nakaoka, S.-I., Niwa, Y., O’Brien, K., Ono, T., Palmer, P. I., Pan, N., Pierrot, D., Pocock,
1077 K., Poulter, B., Resplandy, L., Robertson, E., Rödenbeck, C., Rodriguez, C., Rosan, T. M., Schwinger, J., Séférian, R., Shutler, J. D.,
1078 Skjelvan, I., Steinhoff, T., Sun, Q., Sutton, A. J., Sweeney, C., Takao, S., Tanhua, T., Tans, P. P., Tian, X., Tian, H., Tilbrook, B.,
1079 Tsujino, H., Tubiello, F., van der Werf, G. R., Walker, A. P., Wanninkhof, R., Whitehead, C., Willstrand Wranne, A., et al.: Global
1080 Carbon Budget 2022, *Earth System Science Data*, 14, 4811–4900, 2022.

1081 Gatti, L. V., Basso, L. S., Miller, J. B., Gloor, M., Gatti Domingues, L., Cassol, H. L. G., Tejada, G., Aragão, L. E. O. C., Nobre, C., Peters,
1082 W., Marani, L., Arai, E., Sanches, A. H., Corrêa, S. M., Anderson, L., Von Randow, C., Correia, C. S. C., Crispim, S. P., and Neves,
1083 R. A. L.: Amazonia as a carbon source linked to deforestation and climate change, *Nature*, 595, 388–393, 2021.

1084 Gatti, L. V., Cunha, C. L., Marani, L., Cassol, H. L. G., Messias, C. G., Arai, E., Denning, A. S., Soler, L. S., Almeida, C., Setzer, A.,
1085 Domingues, L. G., Basso, L. S., Miller, J. B., Gloor, M., Correia, C. S. C., Tejada, G., Neves, R. A. L., Rajao, R., Nunes, F., Filho, B.
1086 S. S., Schmitt, J., Nobre, C., Corrêa, S. M., Sanches, A. H., Aragão, L. E. O. C., Anderson, L., Von Randow, C., Crispim, S. P., Silva,
1087 F. M., and Machado, G. B. M.: Increased Amazon carbon emissions mainly from decline in law enforcement, *Nature*, 621, 318–323,
1088 2023.

1089 Grassi, G., Stehfest, E., Rogelj, J., van Vuuren, D., Cescatti, A., House, J., Nabuurs, G.-J., Rossi, S., Alkama, R., Viñas, R. A., Calvin, K.,
1090 Ceccherini, G., Federici, S., Fujimori, S., Gusti, M., Hasegawa, T., Havlik, P., Humpenöder, F., Korosuo, A., Perugini, L., Tubiello,
1091 F. N., and Popp, A.: Critical adjustment of land mitigation pathways for assessing countries’ climate progress, *Nat. Clim. Chang.*, 11,
1092 425–434, 2021.

1093 Grassi, G., Schwingshackl, C., Gasser, T., Houghton, R. A., Sitch, S., Canadell, J. G., Cescatti, A., Ciais, P., Federici, S., Friedlingstein, P.,
1094 Kurz, W. A., Sanz Sanchez, M. J., Abad Viñas, R., Alkama, R., Bultan, S., Ceccherini, G., Falk, S., Kato, E., Kennedy, D., Knauer,

1095 J., Korosuo, A., Melo, J., McGrath, M. J., Nabel, J. E. M. S., Poulter, B., Romanovskaya, A. A., Rossi, S., Tian, H., Walker, A. P.,
1096 Yuan, W., Yue, X., and Pongratz, J.: Harmonising the land-use flux estimates of global models and national inventories for 2000–
1097 2020, *Earth System Science Data*, 15, 1093–1114, 2023.

1098 Hartmann, J., Jansen, N., Dürr, H. H., Kempe, S., and Köhler, P.: Global CO₂-consumption by chemical weathering: What is the
1099 contribution of highly active weathering regions?, *Glob. Planet. Change*, 69, 185–194, 2009.

1100 Höglund-Isaksson, L., Gómez-Sanabria, A., Klimont, Z., Rafaj, P., and Schöpp, W.: Technical potentials and costs for reducing global
1101 anthropogenic methane emissions in the 2050 timeframe –results from the GAINS model, *Environ. Res. Commun.*, 2, 025004, 2020.

1102 IPCC: Revised 1996 IPCC Guidelines for National Greenhouse Inventories, IPCC/OECD/IEA, Paris, France, 1997.

1103 IPCC: 2006 IPCC guidelines for National Greenhouse Gas Inventories, IGES, 2006.

1104 IPCC: 2019 Refinement to the 2006 IPCC Guidelines for National Greenhouse Gas Inventories, edited by: Buendia, E., Tanabe, K., Kranjc,
1105 A., Baasansuren, J., Fukuda, M., Ngarize, S., Osako, A., Pyrozhenko, Y., Shermanau, P., and Federici, S., Intergovernmental Panel
1106 on Climate Change (IPCC), Switzerland, 2019.

1107 IPCC: Climate Change 2023: Synthesis Report, IPCC, Geneva, Switzerland, 2023.

1108 Janardanan, R., Maksyutov, S., Wang, F., Nayagam, L., Sahu, S., Mangaraj, P., Saunio, M., Lan, X., and Matsunaga, T.: Country-level
1109 methane emissions and their sectoral trends during 2009-2020 estimated by high-resolution inversion of GOSAT and surface
1110 observations, *Environmental Research Letters*, 19, 10.1088/1748-9326/ad2436, 2024

1111 Janssens-Maenhout, G., Crippa, M., Guizzardi, D., Muntean, M., Schaaf, E., Dentener, F., Bergamaschi, P., Pagliari, V., Olivier, J. G. J.,
1112 Peters, J. A. H. W., van Aardenne, J. A., Monni, S., Doering, U., Petrescu, A. M. R., Solazzo, E., and Oreggioni, G. D.: EDGAR
1113 v4.3.2 Global Atlas of the three major greenhouse gas emissions for the period 1970–2012, *Earth Syst. Sci. Data*, 11, 959–1002,
1114 2019.

1115 Jin, Z., Wang, T., Zhang, H., Wang, Y., Ding, J., and Tian, X.: Constraint of satellite CO₂ retrieval on the global carbon cycle from a
1116 Chinese atmospheric inversion system, *Sci. China Earth Sci.*, 66, 609–618, 2023.

1117 Jones, M. W., Andrew, R. M., Peters, G. P., Janssens-Maenhout, G., De-Gol, A. J., Dou, X., Liu, Z., Pickers, P., Ciais, P., Patra, P. K.,
1118 Chevallier, F., and Le Quéré, C.: Gridded fossil CO₂ emissions and related O₂ combustion consistent with national inventories, 2022.

1119 Kaminski, T., Rayner, P. J., Heimann, M., and Enting, I. G.: On aggregation errors in atmospheric transport inversions, *J. Geophys. Res. D:*
1120 *Atmos.*, 106, 4703–4715, 2001.

1121 Klein Goldewijk, K., Beusen, A., Doelman, J., and Stehfest, E.: Anthropogenic land use estimates for the Holocene – HYDE 3.2, *Earth*
1122 *Syst. Sci. Data*, 9, 927–953, 2017.

1123 Kong, Y., Zheng, B., Zhang, Q., and He, K.: Global and regional carbon budget for 2015–2020 inferred from OCO-2 based on an
 1124 ensemble Kalman filter coupled with GEOS-Chem, *Atmos. Chem. Phys.*, 22, 10769–10788, 2022.

1125 van der Laan-Luijkx, I. T., van der Velde, I. R., van der Veen, E., Tsuruta, A., Stanislawski, K., Babenhauserheide, A., Zhang, H. F., Liu,
 1126 Y., He, W., Chen, H., Masarie, K. A., Krol, M. C., and Peters, W.: The CarbonTracker Data Assimilation Shell (CTDAS) v1.0:
 1127 implementation and global carbon balance 2001–2015, *Geosci. Model Dev.*, 10, 2785–2800, 2017.

1128 Lauvaux, T., Giron, C., Mazzolini, M., d’Aspremont, A., Duren, R., Cusworth, D., Shindell, D., and Ciais, P.: Global assessment of oil and
 1129 gas methane ultra-emitters, *Science*, 375, 557–561, 2022.

1130 Liu, J., Baskaran, L., Bowman, K., Schimel, D., Bloom, A. A., Parazoo, N. C., Oda, T., Carroll, D., Menemenlis, D., Joiner, J., Commane,
 1131 R., Daube, B., Gatti, L. V., McKain, K., Miller, J., Stephens, B. B., Sweeney, C., and Wofsy, S.: Carbon Monitoring System Flux
 1132 Net Biosphere Exchange 2020 (CMS-Flux NBE 2020), *Earth System Science Data*, 13, 299–330, 2021.

1133 Maksyutov, S., Oda, T., Saito, M., Janardanan, R., Belikov, D., Kaiser, J. W., Zhuravlev, R., Ganshin, A., Valsala, V. K., Andrews, A.,
 1134 Chmura, L., Dlugokencky, E., Haszpra, L., Langenfelds, R. L., Machida, T., Nakazawa, T., Ramonet, M., Sweeney, C., and Worthy,
 1135 D.: Technical note: A high-resolution inverse modelling technique for estimating surface CO₂ fluxes based on the NIES-TM–
 1136 FLEXPART coupled transport model and its adjoint, *Atmos. Chem. Phys.*, 21, 1245–1266, 2021.

1137 Mason Earles, J., Yeh, S., and Skog, K. E.: Timing of carbon emissions from global forest clearance, *Nat. Clim. Chang.*, 2, 682–685, 2012.

1138 Mayorga, E., Seitzinger, S. P., Harrison, J. A., Dumont, E., Beusen, A. H. W., Bouwman, A. F., Fekete, B. M., Kroeze, C., and Van Drecht,
 1139 G.: Global Nutrient Export from WaterSheds 2 (NEWS 2): Model development and implementation, *Environmental Modelling &*
 1140 *Software*, 25, 837–853, 2010.

1141 Naus, S., Domingues, L. G., Krol, M., Luijkx, I. T., Gatti, L. V., Miller, J. B., Gloor, E., Basu, S., Correia, C., Koren, G., Worden, H. M.,
 1142 Flemming, J., Pétron, G., and Peters, W.: Sixteen years of MOPITT satellite data strongly constrain Amazon CO fire emissions,
 1143 *Atmos. Chem. Phys.*, 22, 14735–14750, 2022.

1144 Niwa, Y., Ishijima, K., Ito, A., and Iida, Y.: Toward a long-term atmospheric CO₂ inversion for elucidating natural carbon fluxes:
 1145 technical notes of NISMON-CO₂ v2021.1, *Progress in Earth and Planetary Science*, 9, 1–19, 2022.

1146 Ogle, S. M., Domke, G., Kurz, W. A., Rocha, M. T., Huffman, T., Swan, A., Smith, J. E., Woodall, C., and Krug, T.: Delineating managed
 1147 land for reporting national greenhouse gas emissions and removals to the United Nations framework convention on climate change,
 1148 *Carbon Balance Manag.*, 13, 9, 2018.

1149 Patra, P. K., Takigawa, M., Watanabe, S., Chandra, N., Ishijima, K., and Yamashita, Y.: Improved Chemical Tracer Simulation by
 1150 MIROC4.0-based Atmospheric Chemistry-Transport Model (MIROC4-ACTM), *SOLAIA*, 14, 91–96, 2018.

1151 Patra, P. K., Dlugokencky, E. J., Elkins, J. W., Dutton, G. S., Tohjima, Y., Sasakawa, M., Ito, A., Weiss, R. F., Manizza, M., Krummel, P.
1152 B., Prinn, R. G., O'doherty, S., Bianchi, D., Nevison, C., Solazzo, E., Lee, H., Joo, S., Kort, E. A., Maity, S., and Takigawa, M.:
1153 Forward and Inverse Modelling of Atmospheric Nitrous Oxide Using MIROC4-Atmospheric Chemistry-Transport Model, *Journal of*
1154 *the Meteorological Society of Japan. Ser. II*, 100, 361–386, 2022.

1155 Peng, S., Lin, X., Thompson, R. L., Xi, Y., Liu, G., Hauglustaine, D., Lan, X., Poulter, B., Ramonet, M., Saunio, M., Yin, Y., Zhang, Z.,
1156 Zheng, B., and Ciais, P.: Wetland emission and atmospheric sink changes explain methane growth in 2020, *Nature*, 612, 477–482,
1157 2022.

1158 Perugini, L., Pellis, G., Grassi, G., Ciais, P., Dolman, H., House, J. I., Peters, G. P., Smith, P., Günther, D., and Peylin, P.: Emerging
1159 reporting and verification needs under the Paris Agreement: How can the research community effectively contribute?, *Environ. Sci.*
1160 *Policy*, 122, 116–126, 2021.

1161 Petrescu, A. M. R., McGrath, M. J., Andrew, R. M., Peylin, P., Peters, G. P., Ciais, P., Broquet, G., Tubiello, F. N., Gerbig, C., Pongratz,
1162 J., Janssens-Maenhout, G., Grassi, G., Nabuurs, G.-J., Regnier, P., Lauerwald, R., Kuhnert, M., Balkovič, J., Schelhaas, M.-J., Denier
1163 van der Gon, H. A. C., Solazzo, E., Qiu, C., Pilli, R., Konovalov, I. B., Houghton, R. A., Günther, D., Perugini, L., Crippa, M.,
1164 Ganzenmüller, R., Luijkx, I. T., Smith, P., Munassar, S., Thompson, R. L., Conchedda, G., Monteil, G., Scholze, M., Karstens, U.,
1165 Brockmann, P., and Dolman, A. J.: The consolidated European synthesis of CO₂ emissions and removals for the European Union
1166 and United Kingdom: 1990–2018, *Earth Syst. Sci. Data*, 13, 2363–2406, 2021.

1167 Philibert, A., Loyce, C., and Makowski, D.: Prediction of N₂O emission from local information with Random Forest, *Environ. Pollut.*, 177,
1168 156–163, 2013.

1169 Potapov, P., Hansen, M. C., Laestadius, L., Turubanova, S., Yaroshenko, A., Thies, C., Smith, W., Zhuravleva, I., Komarova, A.,
1170 Minnemeyer, S., and Esipova, E.: The last frontiers of wilderness: Tracking loss of intact forest landscapes from 2000 to 2013, *Sci*
1171 *Adv*, 3, e1600821, 2017.

1172 Regnier, P., Friedlingstein, P., Ciais, P., Mackenzie, F. T., Gruber, N., Janssens, I. A., Laruelle, G. G., Lauerwald, R., Luysaert, S.,
1173 Andersson, A. J., Arndt, S., Arnosti, C., Borges, A. V., Dale, A. W., Gallego-Sala, A., Goddérís, Y., Goossens, N., Hartmann, J.,
1174 Heinze, C., Ilyina, T., Joos, F., LaRowe, D. E., Leifeld, J., Meysman, F. J. R., Munhoven, G., Raymond, P. A., Spahni, R.,
1175 Suntharalingam, P., and Thullner, M.: Anthropogenic perturbation of the carbon fluxes from land to ocean, *Nat. Geosci.*, 6, 597–607,
1176 2013.

1177 Rödenbeck, C., Houweling, S., Gloor, M., and Heimann, M.: CO₂ flux history 1982–2001 inferred from atmospheric data using a global
1178 inversion of atmospheric transport, *Atmos. Chem. Phys.*, 3, 1919–1964, 2003.

1179 Sauniois, M., Stavert, A. R., Poulter, B., Bousquet, P., Canadell, J. G., Jackson, R. B., Raymond, P. A., Dlugokencky, E. J., Houweling, S.,
1180 Patra, P. K., Ciais, P., Arora, V. K., Bastviken, D., Bergamaschi, P., Blake, D. R., Brailsford, G., Bruhwiler, L., Carlson, K. M.,
1181 Carrol, M., Castaldi, S., Chandra, N., Crevoisier, C., Crill, P. M., Covey, K., Curry, C. L., Etiope, G., Frankenberg, C., Gedney, N.,
1182 Hegglin, M. I., Höglund-Isaksson, L., Hugelius, G., Ishizawa, M., Ito, A., Janssens-Maenhout, G., Jensen, K. M., Joos, F., Kleinen,
1183 T., Krummel, P. B., Langenfelds, R. L., Laruelle, G. G., Liu, L., Machida, T., Maksyutov, S., McDonald, K. C., McNorton, J., Miller,
1184 P. A., Melton, J. R., Morino, I., Müller, J., Murguia-Flores, F., Naik, V., Niwa, Y., Noce, S., O'Doherty, S., Parker, R. J., Peng, C.,
1185 Peng, S., Peters, G. P., Prigent, C., Prinn, R., Ramonet, M., Regnier, P., Riley, W. J., Rosentreter, J. A., Segers, A., Simpson, I. J.,
1186 Shi, H., Smith, S. J., Steele, L. P., Thornton, B. F., Tian, H., Tohjima, Y., Tubiello, F. N., Tsuruta, A., Viovy, N., Voulgarakis, A.,
1187 Weber, T. S., van Weele, M., van der Werf, G. R., Weiss, R. F., Worthy, D., Wunch, D., Yin, Y., Yoshida, Y., Zhang, W., Zhang, Z.,
1188 Zhao, Y., Zheng, B., Zhu, Q., Zhu, Q., and Zhuang, Q.: The global methane budget 2000–2017, *Earth Syst. Sci. Data*, 12, 1561–1623,
1189 2020.

1190 [Sauniois, M., Martinez, A., Poulter, B., Zhang, Z., Raymond, P., Regnier, P., Canadell, J. G., Jackson, R. B., Patra, P. K., Bousquet, P.,](#)
1191 [Ciais, P., Dlugokencky, E. J., Lan, X., Allen, G. H., Bastviken, D., Beerling, D. J., Belikov, D. A., Blake, D. R., Castaldi, S., Crippa,](#)
1192 [M., Deemer, B. R., Dennison, F., Etiope, G., Gedney, N., Höglund-Isaksson, L., Holgerson, M. A., Hopcroft, P. O., Hugelius, G., Ito,](#)
1193 [A., Jain, A. K., Janardanan, R., Johnson, M. S., Kleinen, T., Krummel, P., Lauerwald, R., Li, T., Liu, X., McDonald, K. C., Melton, J.](#)
1194 [R., Mühle, J., Müller, J., Murguia-Flores, F., Niwa, Y., Noce, S., Pan, S., Parker, R. J., Peng, C., Ramonet, M., Riley, W. J., Rocher-](#)
1195 [Ros, G., Rosentreter, J. A., Sasakawa, M., Segers, A., Smith, S. J., Stanley, E. H., Thanwerdas, J., Tian, H., Tsuruta, A., Tubiello, F.](#)
1196 [N., Weber, T. S., van der Werf, G., Worthy, D. E., Xi, Y., Yoshida, Y., Zhang, W., Zheng, B., Zhu, Q., Zhu, Q., and Zhuang, Q.:](#)
1197 [Global Methane Budget 2000–2020, *Earth Syst. Sci. Data Discuss.* \[preprint\], <https://doi.org/10.5194/essd-2024-115>, in review,](#)
1198 [2024.](#)

1199 Schuldt, K. N., Mund, J., Lujikx, I. T., Aalto, T., Abshire, J. B., Aikin, K., Andrews, A., Aoki, S., Apadula, F., Baier, B., Bakwin, P.,
1200 Bartyzel, J., Bentz, G., Bergamaschi, P., Beyersdorf, A., Biermann, T., Biraud, S. C., Boenisch, H., Bowling, D., Brailsford, G., van
1201 den Bulk, P., Chen, G., Chen, H., Chmura, L., Clark, S., Climadat, S., Della Coletta, J., Colomb, A., Commane, R., Conil, S., Cox, A.,
1202 Cristofanelli, P., Cuevas, E., Curcoll, R., Daube, B., Davis, K., Delmotte, M., DiGangi, J. P., van Dinter, D., Dlugokencky, E.,
1203 Elkins, J. W., Emmenegger, L., Fang, S., Fischer, M. L., Forster, G., Frumau, A., Galkowski, M., Gatti, L. V., Gehrlein, T., Gerbig,
1204 C., Gheusi, F., Gloor, E., Gomez-Trueba, V., Goto, D., Griffis, T., Hammer, S., Hanson, C., Haszpra, L., Hatakka, J., Heimann, M.,
1205 Heliasz, M., Hensen, A., Hermanssen, O., Hintsa, E., Holst, J., Ivakhov, V., Jaffe, D., Joubert, W., Karion, A., Kawa, S. R., Kazan,
1206 V., Keeling, R., Keronen, P., Kolari, P., Kominkova, K., Kort, E., Kozlova, E., Krummel, P., Kubistin, D., Labuschagne, C., Lam, D.

1207 H. Y., Langenfelds, R., Laurent, O., Laurila, T., Lauvaux, T., Lavric, J., Law, B., Lee, J., Lee, O. S. M., Lehner, I., Leppert, R.,
1208 Leuenberger, M., Levin, I., Levula, J., Lin, J., Lindauer, M., Loh, Z., Lopez, M., Machida, T., et al.: Multi-laboratory compilation of
1209 atmospheric carbon dioxide data for the period 1957-2020; obspack_co2_1_GLOBALVIEWplus_v7.0_2021-08-18, 2021.

1210 Schuldts, K. N., Jacobson, A. R., Aalto, T., Andrews, A., Bakwin, P., Bergamaschi, P., Biermann, T., Biraud, S. C., Chen, H., Colomb, A.,
1211 Conil, S., Cristofanelli, P., Delmotte, M., Dlugokencky, E., Emmenegger, L., Fischer, M. L., Hatakka, J., Heliasz, M., Hermanssen,
1212 O., Holst, J., Jaffe, D., Karion, A., Kazan, V., Keronen, P., Kominkova, K., Kubistin, D., Laurent, O., Laurila, T., Lee, J., Lehner, I.,
1213 Leuenberger, M., Lindauer, M., Lopez, M., Mammarella, I., Manca, G., Marek, M. V., De Mazière, M., McKain, K., Miller, C. E.,
1214 Miller, J. B., Mölder, M., Müller-Williams, J., Myhre, C. L., Piacentino, S., Pichon, J. M., Plass-Duelmer, C., Plass-Duelmer, C.,
1215 Ramonet, M., di Sarra, A. G., Scheeren, B., Schumacher, M., Sha, M. K., Sloop, C. D., Smith, P., Steinbacher, M., Sweeney, C.,
1216 Tans, P., Thoning, K., Tørseth, K., Trisolino, P., Viner, B., Vitkova, G., and De Wekker, S.: Multi-laboratory compilation of
1217 atmospheric carbon dioxide data for the year 2022; obspack_co2_1_NRT_v7.2_2022-06-28, 2022.

1218 Segers, A. and Houweling, S.: Description of the CH₄ Inversion Production Chain, Copernicus Atmosphere Monitoring Service, 2017.

1219 Shcherbak, I., Millar, N., and Robertson, G. P.: Global metaanalysis of the nonlinear response of soil nitrous oxide (N₂O) emissions to
1220 fertilizer nitrogen, *Proc. Natl. Acad. Sci. U. S. A.*, 111, 9199–9204, 2014.

1221 Thompson, R. L., Chevallier, F., Crotwell, A. M., Dutton, G., Langenfelds, R. L., Prinn, R. G., Weiss, R. F., Tohjima, Y., Nakazawa, T.,
1222 Krummel, P. B., Steele, L. P., Fraser, P., O’Doherty, S., Ishijima, K., and Aoki, S.: Nitrous oxide emissions 1999 to 2009 from a
1223 global atmospheric inversion, *Atmos. Chem. Phys.*, 14, 1801–1817, 2014.

1224 Tian, H., Yang, J., Xu, R., Lu, C., Canadell, J. G., Davidson, E. A., Jackson, R. B., Arneeth, A., Chang, J., Ciais, P., Gerber, S., Ito, A., Joos,
1225 F., Lienert, S., Messina, P., Olin, S., Pan, S., Peng, C., Saikawa, E., Thompson, R. L., Vuichard, N., Winiwarter, W., Zaehle, S., and
1226 Zhang, B.: Global soil nitrous oxide emissions since the preindustrial era estimated by an ensemble of terrestrial biosphere models:
1227 Magnitude, attribution, and uncertainty, *Glob. Chang. Biol.*, 25, 640–659, 2019.

1228 Tian, H., Xu, R., Canadell, J. G., Thompson, R. L., Winiwarter, W., Suntharalingam, P., Davidson, E. A., Ciais, P., Jackson, R. B.,
1229 Janssens-Maenhout, G., Prather, M. J., Regnier, P., Pan, N., Pan, S., Peters, G. P., Shi, H., Tubiello, F. N., Zaehle, S., Zhou, F.,
1230 Arneeth, A., Battaglia, G., Berthet, S., Bopp, L., Bouwman, A. F., Buitenhuis, E. T., Chang, J., Chipperfield, M. P., Dangal, S. R. S.,
1231 Dlugokencky, E., Elkins, J. W., Eyre, B. D., Fu, B., Hall, B., Ito, A., Joos, F., Krummel, P. B., Landolfi, A., Laruelle, G. G.,
1232 Lauerwald, R., Li, W., Lienert, S., Maavara, T., MacLeod, M., Millet, D. B., Olin, S., Patra, P. K., Prinn, R. G., Raymond, P. A.,
1233 Ruiz, D. J., van der Werf, G. R., Vuichard, N., Wang, J., Weiss, R. F., Wells, K. C., Wilson, C., Yang, J., and Yao, Y.: A
1234 comprehensive quantification of global nitrous oxide sources and sinks, *Nature*, 586, 248–256, 2020.

1235 Tian, H., Pan, N., Thompson, R. L., Canadell, J. G., Suntharalingam, P., Regnier, P., Davidson, E. A., Prather, M., Ciais, P., Muntean, M.,
1236 Pan, S., Winiwarter, W., Zaehle, S., Zhou, F., Jackson, R. B., Bange, H. W., Berthet, S., Bian, Z., Bianchi, D., Bouwman, A. F.,
1237 Buitenhuis, E. T., Dutton, G., Hu, M., Ito, A., Jain, A. K., Jeltsch-Thömmes, A., Joos, F., Kou-Giesbrecht, S., Krummel, P. B., Lan,
1238 X., Landolfi, A., Lauerwald, R., Li, Y., Lu, C., Maavara, T., Manizza, M., Millet, D. B., Mühle, J., Patra, P. K., Peters, G. P., Qin, X.,
1239 Raymond, P., Resplandy, L., Rosentreter, J. A., Shi, H., Sun, Q., Tonina, D., Tubiello, F. N., van der Werf, G. R., Vuichard, N.,
1240 Wang, J., Wells, K. C., Western, L. M., Wilson, C., Yang, J., Yao, Y., You, Y., and Zhu, Q.: Global Nitrous Oxide Budget 1980–
1241 2020, *Earth System Science Data Discussions*, 1–98, 2023.

1242 Tibrewal, K., Ciais, P., Saunois, M., Martinez, A., Lin, X., Thanwerdas, J., Deng, Z., Chevallier, F., Giron, C., Albergel, C., Tanaka, K.,
1243 Patra, P., Tsuruta, A., Zheng, B., Belikov, D., Niwa, Y., Janardanan, R., Maksyutov, S., Segers, A., Tzompa-Sosa, Z. A., Bousquet,
1244 P., and Sciare, J.: Assessment of methane emissions from oil, gas and coal sectors across inventories and atmospheric inversions,
1245 *Commun. Earth Environ.*, 5, <https://doi.org/10.1038/s43247-023-01190-w>, 2024.

1246 Tsuruta, A., Aalto, T., Backman, L., Hakkarainen, J., van der Laan-Luijkx, I. T., Krol, M. C., Spahni, R., Houweling, S., Laine, M.,
1247 Dlugokencky, E., Gomez-Pelaez, A. J., van der Schoot, M., Langenfelds, R., Ellul, R., Arduini, J., Apadula, F., Gerbig, C., Feist, D.
1248 G., Kivi, R., Yoshida, Y., and Peters, W.: Global methane emission estimates for 2000–2012 from CarbonTracker Europe-CH4 v1.0,
1249 *Geosci. Model Dev.*, 10, 1261–1289, 2017.

1250 UNFCCC: Biennial Update Report submissions from Non-Annex I Parties, available at: <https://unfccc.int/BURs>, last access: 2 July 2021a.

1251 UNFCCC: National Communication submissions from Non-Annex I Parties, available at: <https://unfccc.int/non-annex-I-NCs>, last access:
1252 5 December 2021b.

1253 Wang, J. A., Baccini, A., Farina, M., Randerson, J. T., and Friedl, M. A.: Disturbance suppresses the aboveground carbon sink in North
1254 American boreal forests, *Nat. Clim. Chang.*, 11, 435–441, 2021.

1255 Wang, Q., Zhou, F., Shang, Z., Ciais, P., Winiwarter, W., Jackson, R. B., Tubiello, F. N., Janssens-Maenhout, G., Tian, H., Cui, X.,
1256 Canadell, J. G., Piao, S., and Tao, S.: Data-driven estimates of global nitrous oxide emissions from croplands, *Natl Sci Rev*, 7, 441–
1257 452, 2020.

1258 van Wees, D., van der Werf, G. R., Randerson, J. T., Rogers, B. M., Chen, Y., Veraverbeke, S., Giglio, L., and Morton, D. C.: Global
1259 biomass burning fuel consumption and emissions at 500 m spatial resolution based on the Global Fire Emissions Database (GFED),
1260 *Geoscientific Model Development*, 15, 8411–8437, 2022.

1261 Wells, K. C., Millet, D. B., Bousseres, N., Henze, D. K., Chaliyakunnel, S., Griffis, T. J., Luan, Y., Dlugokencky, E. J., Prinn, R. G.,
1262 O’Doherty, S., Weiss, R. F., Dutton, G. S., Elkins, J. W., Krummel, P. B., Langenfelds, R., Steele, L. P., Kort, E. A., Wofsy, S. C.,

删除[Shamil]: Wang, F., Maksyutov, S., Tsuruta, A.,
Janardanan, R., Ito, A., Sasakawa, M., Machida, T., Morino, I.,
Yoshida, Y., Kaiser, J. W., Janssens-Maenhout, G.,
Dlugokencky, E. J., Mammarella, I., Lavric, J. V., and
Matsunaga, T.: Methane Emission Estimates by the Global
High-Resolution Inverse Model Using National Inventories,
Remote Sensing, 11, 2489, 2019.

删除[Shamil]:

1263 and Umezawa, T.: Simulation of atmospheric N₂O with GEOS-Chem and its adjoint: evaluation of observational constraints, *Geosci.*
1264 *Model Dev.*, 8, 3179–3198, 2015.

1265 Wilson, C., Chipperfield, M. P., Gloor, M., and Chevallier, F.: Development of a variational flux inversion system (INVICAT v1.0) using
1266 the TOMCAT chemical transport model, *Geosci. Model Dev.*, 7, 2485–2500, 2014.

1267 Winkler, K., Yang, H., Ganzenmüller, R., Fuchs, R., Ceccherini, G., Duveiller, G., Grassi, G., Pongratz, J., Bastos, A., Shvidenko, A.,
1268 Araza, A., Herold, M., Wigneron, J.-P., and Ciais, P.: Changes in land use and management led to a decline in Eastern Europe’s
1269 terrestrial carbon sink, *Communications Earth & Environment*, 4, 1–14, 2023.

1270 Xu, X., Sharma, P., Shu, S., Lin, T.-S., Ciais, P., Tubiello, F. N., Smith, P., Campbell, N., and Jain, A. K.: Global Greenhouse Gas
1271 Emissions from Plant-and Animal-Based Food, *Nature Food*, 2021.

1272 Yao, Y., Tian, H., Shi, H., Pan, S., Xu, R., Pan, N., and Canadell, J. G.: Increased global nitrous oxide emissions from streams and rivers
1273 in the Anthropocene, *Nat. Clim. Chang.*, 10, 138–142, 2019.

1274 Yin, Y., Chevallier, F., Ciais, P., Broquet, G., Fortems-Cheiney, A., Pison, I., and Saunois, M.: Decadal trends in global CO emissions as
1275 seen by MOPITT, *Atmos. Chem. Phys.*, 15, 13433–13451, 2015.

1276 Zheng, B., Chevallier, F., Ciais, P., Yin, Y., Deeter, M. N., Worden, H. M., Wang, Y., Zhang, Q., and He, K.: Rapid decline in carbon
1277 monoxide emissions and export from East Asia between years 2005 and 2016, *Environ. Res. Lett.*, 13, 044007, 2018.

1278 Zhou, F., Shang, Z., Zeng, Z., Piao, S., Ciais, P., Raymond, P. A., Wang, X., Wang, R., Chen, M., Yang, C., Tao, S., Zhao, Y., Meng, Q.,
1279 Gao, S., and Mao, Q.: New model for capturing the variations of fertilizer-induced emission factors of N₂O, *Global Biogeochem.*
1280 *Cycles*, 29, 885–897, 2015.

1281 Zscheischler, J., Mahecha, M. D., Avitabile, V., Calle, L., Carvalhais, N., Ciais, P., Gans, F., Gruber, N., Hartmann, J., Herold, M., Ichii,
1282 K., Jung, M., Landschützer, P., Laruelle, G. G., Lauerwald, R., Papale, D., Peylin, P., Poulter, B., Ray, D., Regnier, P., Rödenbeck,
1283 C., Roman-Cuesta, R. M., Schwalm, C., Tramontana, G., Tyukavina, A., Valentini, R., van der Werf, G., West, T. O., Wolf, J. E.,
1284 and Reichstein, M.: Reviews and syntheses: An empirical spatiotemporal description of the global surface–atmosphere carbon fluxes:
1285 opportunities and data limitations, *Biogeosciences*, 14, 3685–3703, 2017.

删除[Zhu Deng]: